RESEARCH ARTICLE

RUNNING HEAD: Partial correction of F508del-CFTR thermal instability

Effect of elexacaftor and bamocaftor on the metabolic and thermal stability of the F508del-CFTR protein in human airway epithelial cells

Thomas Carrez [1,2], Sandra Mirval [1], Christine Barrault[1], Florian Devetter[1], Clarisse Vandebrouck[1], and Frédéric Becq [1*]

[1]Laboratoire de physiopathologie et régulation des transports ioniques, Pôle Biologie Santé, Université de Poitiers, 86073 Poitiers, France

[2]ManRos Therapeutics, Hôtel de Recherche, Presqu'île de Perharidy, 29680 Roscoff, France.

* **Address correspondence to:**
Prof. Frédéric Becq
Laboratoire de Physiopathologie et Régulation des Transports Ioniques,
Université de Poitiers, Bâtiment Pôle Biologie Santé,
1 rue Georges Bonnet, 86073, Poitiers, France.
Phone : (33) 549453729
Email : frederic.becq@univ-poitiers.fr

ABSTRACT

Trikafta (elexacaftor/tezacaftor/ivacaftor, ETI) is approved for cystic fibrosis (CF) patients with at least one F508del mutation in the CFTR gene or another responsive mutation based on *in vitro* data. However, the pharmacological effects of ETI on F508del-CFTR remain incompletely defined in vitro. To explore the mechanisms underlying Trikafta's clinical efficacy, we used primary bronchial epithelial cells from F508del homozygous patients and CFBE41o- cells expressing F508del-CFTR. We assessed CFTR maturation, turnover, chloride transport, and thermal stability under various ETI concentrations and treatment durations at physiological temperature using electrophysiology (Ussing chamber, patch-clamp) and biochemical assays. We found that ETI efficacy on F508del-CFTR is strongly influenced by both treatment duration and concentration. Reducing ETI from standard doses, i.e. E (3 μM), T (18 μM), I (1 μM), to 33%, 11%, 3.3%, and 1.1% decreased function and maturation, but 33% retained most of the corrective effect. After 2 hours of treatment, around 50% of the CFTR-dependent current was preserved, unlike in untreated cells. Notably, replacing elexacaftor with bamocaftor further improved F508del-CFTR maturation and function compared to ETI, though it did not affect the rate of current decline over time. These findings highlight the importance of optimizing ETI dose and exposure duration, as both significantly affect F508del-CFTR stability and function. The retained efficacy at reduced concentrations suggests possible individualized dosing strategies, particularly for patients experiencing adverse effects with full-dose ETI.

NEW & NOTEWORTHY

Our *in vitro* study underscores that ETI/BTI's efficacy in improving F508del-CFTR function depends on treatment concentration and duration, impacting the protein's metabolic and thermal stability. Although ETI/BTI only partially addresses F508del-CFTR's inherent thermal instability, reduced doses retained significant effectiveness. This finding supports dose optimization as a promising strategy to sustain therapeutic benefits while minimizing side effects, offering a personalized approach to treatment for individuals with cystic fibrosis experiencing adverse effects from standard dosing.

Keywords: Cystic Fibrosis, F508del-CFTR, thermal instability, elexacaftor, bamocaftor, dose reduction

INTRODUCTION

Cystic Fibrosis (CF) is an autosomal recessive disorder caused by loss-of-function mutations in the gene encoding the Cystic Fibrosis Transmembrane Conductance Regulator (CFTR) protein (1-4). This life-shortening disease affects multiple organs, including the lungs, intestines, exocrine pancreas, biliary tree, sinuses, and vas deferens. CFTR is a phosphorylation-dependent, ligand-gated chloride channel that belongs to the ATP-binding cassette (ABC) transporter family, and it is expressed at the apical plasma membrane of epithelial cells (4, 5). CFTR channel activation requires phosphorylation, typically by PKA, and ATP binding. Structurally, CFTR consists of two transmembrane domains (TMD1 and TMD2), two nucleotide-binding domains (NBD1 and NBD2), and a regulatory domain (R) (1,6). This configuration allows the transport of chloride and bicarbonate ions across epithelial cells, crucial for airway surface liquid homeostasis, hydration, and pH regulation (7). The F508del mutation is the most common pathogenic variant of CFTR, resulting in multiple defects in protein structure and function (1-4). This variant is characterized by defective processing and intracellular transport, leading to reduced expression at the plasma membrane (8). Additionally, F508del-CFTR exhibits impaired channel gating (9), reduced plasma membrane stability with accelerated recycling (10), and increased thermal instability at physiological temperatures (11-15).

Pharmacological interventions, chemical chaperones, and proteostasis modulators have shown limited success in fully rescuing the function of defective CFTR proteins (16-18). Although comprehensive correction of F508del-CFTR defects remains elusive, the highly effective CFTR modulator therapy (HEMT) ETI (elexacaftor, tezacaftor, and ivacaftor), known commercially as Trikafta® (named Kaftrio® in Europe) is approved for patients 6 years and older in many regions (e.g., U.S., EU). It is prescribed for CF people (pwCF) with at least one F508del mutation in the CFTR gene, including F508del/F508del (homozygous), F508del/another responsive CF-causing mutation based on *in vitro* data (heterozygous, one of 177 other CFTR mutations, see also www.trikafta.com) (19-21). Trikafta includes two correctors, elexacaftor and tezacaftor (VX445 and VX661, respectively), which improve the folding, trafficking, and maturation of the defective CFTR protein (16-18), allowing it to reach the apical membrane where it exhibits partial functionality due to intrinsic gating defects. To enhance channel activity, the potentiator ivacaftor (VX770) is included (22, 23). Elexacaftor also acts as a dual corrector and potentiator, increasing CFTR open probability (24-26). A second corrector, bamocaftor (VX-659), when combined with tezacaftor and

ivacaftor (hereafter named BTI), demonstrated robust *in vitro* and *in vivo* activity, resulting in significant clinical improvements for pwCF (27). However, the therapeutic development of products containing bamocaftor was discontinued (as reported on the CFF and Vertex websites) in favor of a combination involving elexacaftor. This shift ultimately led to the development and marketing of Trikafta®.

Correctors are categorized based on their binding sites on CFTR, as revealed by recent structural studies (28). These sites are grouped into three classes: C1 correctors (e.g., VX809 and VX661), which stabilize NBD1-MSD1 (29) and NBD1-MSD2 interfaces, as well as NBD1 interactions with intracellular loops 1 and 4 (30-33); C2 correctors (e.g., Corr-4a), can stabilize NBD2 and its interfaces (18); and C3 correctors (e.g., VX445), which stabilize NBD1 (28). The combined action of these modulators in Trikafta effectively rescues both the function and structure of F508del-CFTR through complementary domain binding (6, 28). Ivacaftor, the potentiator, has been proposed to bind within a cleft formed by transmembrane helices 4, 5, and 8, at the protein-lipid interface (25), although other binding sites, such as cytosolic loop 4, may also exist (34).

The thermal instability of F508del-CFTR negatively affects its expression, function, and residence at the plasma membrane (11-15). While ivacaftor enhances channel conductance, it can accelerate CFTR turnover and reduce the efficacy of correctors when used alone (35-37). In this study, we utilized human (F508del/F508del) bronchial epithelial cells and CFBE41o- cell lines expressing F508del- or wild-type CFTR to examine the effects of ETI/BTI on the effective incubation time and concentration-dependent rescue of F508del-CFTR function, maturation, and metabolic stability. Additionally, we investigated how ETI/BTI influences the thermal inactivation of F508del-CFTR through long-term transepithelial current recordings at 37°C, an aspect not previously explored.

MATERIALS AND METHODS

Cell culture and cell treatments

Primary cell cultures were established from 3 F508del homozygous female donors (aged 23-31) allowing human F508del bronchial epithelial (CF-HBE) cells preparations obtained post-lung transplantation (Foch Hospital, Suresnes, France). Detailed collection methods and protocols are described elsewhere (15, 37). The primary CF-HBE cell cultures were seeded in dishes using PneumaCult™-Ex medium (StemCell Technologies, France) as the proliferation medium. Human bronchial epithelial cell lines CFBE41o- expressing wild-type CFTR and

CFBE41o- expressing F508del-CFTR were provided by Dr. D. Gruenert (University of California, San Francisco, USA). These cell lines were maintained at 37°C in a 5% CO_2 and 95% air environment, with the culture media refreshed every 2 days. Cells were cultured in Eagle's Minimum Essential Medium (EMEM) supplemented with non-essential amino acids (Gibco), 10% fetal bovine serum (Eurobio), 2 mM L-glutamine (Gibco), and antibiotics (50 IU/mL penicillin and 50 µg/mL streptomycin, Sigma-Aldrich). Selection was performed using 5 µg/mL puromycin (Gibco).

To assess the effects of the triple combination therapy elexacaftor (or bamocaftor) /tezacaftor/ivacaftor (ETI), cells expressing F508del-CFTR were treated for durations ranging from 2 to 24 hours before experimentation. The treatment concentrations were as follows (except where noted): 3 µM elexacaftor, 0–18 µM tezacaftor, and 1 µM ivacaftor (Selleck Chemicals, USA). Bamocaftor (Selleck Chemicals, USA) was used at 3 µM. Stock solutions were prepared at a minimum 1000-fold concentration in DMSO, ensuring that the final DMSO concentration during cell treatment did not exceed 0.1% (v/v).

Short-circuit current measurements

Cells were seeded at a density of 0.5 x 10^6 cells (CFBE41o-) or 0.2 x 10^6 cells (CF-HBE) on Snapwell permeable inserts (Corning corp.) coated with human fibronectine (CFBE41o-, 5 µg.cm^{-2}; Sigma Aldrich) or ColIagene IV (CF-HBE, 16µg/cm^2 ; C7521, Sigma Aldrich). After 2 days at liquid/liquid interface, cells were cultured at the air/liquid interface interface and culture media were renewed every 2 or 3 days, Eagle's minimum essential medium complete medium without puromycin for CFBE cell line and Pneumacult™-ALI culture medium (StemCell Technologies, France) for CF-HBE cells. Inserts were mounted in an EM-CSYS-6 Ussing chamber system (Physiologic Instruments Inc., USA) made of two hemi-chambers, each containing the following solutions (in mM): 1.2 NaCl, 115 Na-gluconate, 25 $NaHCO_3$, 1.2 $MgCl_2$, 4 $CaCl_2$, 2.4 KH_2PO_4, 1.24 K_2HPO_4, 10 mannitol (pH 7.4) for low Cl^- apical solution and 115 NaCl, 25 $NaHCO_3$, 1.2 $MgCl_2$, 1.2 $CaCl_2$, 2.4 KH_2PO_4, 1.24 K_2HPO_4, 10 glucose (pH 7.4) for basolateral solution. We used these asymmetric solutions to create a basal to apical chloride gradient (15, 37). Both solutions were maintained at 37°C (controlled before, during and after each experiment) and gassed with 95% oxygen–5% CO_2. Transepithelial potential difference and short-circuit currents (Isc) were measured/injected through 3M KCl filled Ag/AgCl electrodes connected to a VCC MC voltage/current clamp (Physiologic Instruments Inc., USA). We visualized and recorded the current injected by the system to short-circuit pseudoepithelia (clamp at 0 mV), at a frequency of 0.1 Hz, on a

personal computer using Acquire and Analyze hardware and software (Physiologic Instruments Inc., USA). Transepithelial potential difference values were corrected for the junction potential between apical and basal solutions and for empty insert resistance. Since the polarity of Isc was referred to the basolateral side of the pseudo-epithelium and a gain of -10 was applied, an apical anion secretion is indicated by an upward deflection of the signal meaning increase in Isc. The following drugs were added in the apical chamber: amiloride (Sigma Aldrich, 100 μM from 100 mM DMSO stock) to inhibit ENaC currents, forskolin (Sigma Aldrich, 1 to 10 μM from 1 or 10 mM DMSO stock) to stimulate CFTR-dependent currents, and $CFTRinh_{172}$ (MedChemExpress, 10 μM from 10 mM DMSO stock) to selectively inhibit CFTR-dependent currents (38), apical UTP (Sigma Aldrich, Uridine 5' triphosphate, 100 μM from 100 mM in water stock) to stimulate CaCCs and it includes purinergic-dependent currents mediated by the TMEM16a calcium-dependent chloride channel. We added UTP after complete CFTR inhibition. In some experiments we also added VX770 (MedChemExpress, 1 μM from 10 mM DMSO stock) to further potentiate the CFTR activity after forskolin addition. Solution temperature was controlled with a digital precision thermometer (Checktemp®1, Hanna Instruments, USA) placed directly into each hemi-chamber of the Ussing chamber setup before, during and after each recording for each insert. For experiments at physiological or near physiological temperatures, results were discarded when temperature varied by more than 1°C above or below the desired temperature (15).

Patch clamp experiments

We employed an automated whole-cell patch clamp (APC) technique using the 8-channel Patchliner NPC-16 workstation (Nanion Technologies GmbH, Munich, Germany) integrated with two QuadroEPC-10 amplifiers (HEKA Elektronik GmbH, Germany) (15, 37). Membrane potential pulses were delivered from a holding potential of -40 mV to test potentials ranging from −80 to +80 mV in 20 mV increments to generate current density/voltage data. The external bath solution was composed of (in mM): 145 NMDG, 145 HCl, 10 TES, 5 $BaCl_2$, 2 $CaCl_2$, and 2 $MgCl_2$, adjusted to pH 7.4 using NMDG, with an osmolarity of 300 ± 10 mOsmol. The internal pipette solution contained (in mM): 105 NMDG, 30 H_2SO_4, 20 HCl, 10 TES, 10 EGTA, 4 $MgCl_2$, and 3 MgATP, adjusted to pH 7.2 using HCl, with an osmolarity of 285 ± 5 mOsmol. The theoretical E_{Cl-} was calculated as −44 mV using the Nernst equation. Recordings were conducted at room temperature (20-25°C) and analyzed with Patch MasterPro software (HEKA) and Igor software. The CFTR current

was activated by forskolin (10 µM, Sigma Aldrich, USA) and genistein (30 µM, Sigma Aldrich, USA) and inhibited by $CFTRinh_{172}$ (10 µM, MedChemExpress, USA).

Western blot

CFBE41o- F508del-CFTR and WT were lysed on ice (lysed buffer: 10 mM Tris HCl, 1% Nonidet P-40, 0.5% sodium deoxycholate, 1 mM de Pefabloc® SC (Sigma Aldrich, Germany), 1 mM protease inhibitors cocktail (Roche, Germany), 1 mM phosphatase inhibitor (Roche, Germany); pH 7.5). Extracted protein was quantified using a BCA kit (Pierce, Thermo Scientific, USA) and 30 µg protein samples were separated on sodium dodecyl sulphate–polyacrylamide gel electrophoresis (SDS-PAGE) (8%) and transferred to a nitrocellulose membrane. The membrane was subjected to Western blotting using a mouse anti-CFTR antibody (1:1000; antibody CF596 obtained from the CF Foundation), a mouse anti-GAPDH (1:1000; Sc-32233 Santa Cruz). Horseradish peroxidase-conjugated goat anti-mouse antibody (1:10000, Sigma Aldrich, Germany), goat anti-rabbit antibody (1:10000, Sigma Aldrich, Germany) were used as secondary antibody, and proteins were detected using enhanced chemiluminescence (Immobilon; Merck Millipore, France). Images were obtained using the GeneGnome Imager (SynGene Ozyme, France) and analysed for densitometry with the Genetools software (SynGene Ozyme, France). We normalized the intensity of the CFTR bands B and C to GAPDH, our loading control. CFTR maturation status was estimated by the band C/(band B+band C) ratio. We used the Page Ruler pre-stained protein ladder (Thermo Scientific, USA) and Blue Star pre-stained protein marker (MWP04, Genetics) to identify the molecular weight of proteins on SDS-polyacrylamide gels. To evaluate CFTR half-life, CFBE41o- F508del-CFTR and WT cells were treated with cycloheximide (CHX: 100 µg/mL) at different time points (0-24h). Then, cells were lysed with the same lysis buffer as described above and the same procedures used for SDS-PAGE were followed.

Statistical analysis

Data are presented as mean ± SD of *n* observations. For CFBE41o- cells, n represents the number of replicates performed on different cell cultures and different days. For HBE cells, n refers to measurements using cells from the same donor on different days. Sample sizes (n) and exact p value are noted in figures and legends except for $p<0.0001$ indicated by the symbol ****. Statistical comparisons were made using non-parametric ($n < 10$) or parametric ($n \geq 10$) tests with a significance level of 0.05. Before using a parametric test, samples were checked

for normality using Shapiro-Wilk normality test. Statistical significance of differences between two conditions in a same group was calculated using a student's t-test (parametric) or a Mann-Whitney test (non-parametric). If more than two conditions are compared, a one-way analysis of variance (ANOVA) followed by a Fisher test was used. All statistics analysis were made by GraphPad Prism version 6.0 (GraphPad Software, San Diego, CA, USA) software.

RESULTS

Effect of ETI treatment F508del-CFTR Isc in human bronchial epithelial cells F508del/F508del

Our assay protocol for recording the activation and inhibition of ETI-corrected F508del-CFTR-mediated Isc is illustrated in Figure S1A. The total increase in CFTR-dependent Isc (hereafter referred to as ΔIsc) upon activation represents the current stimulated by forskolin and enhanced by ivacaftor in experiments using ET- and ETI-treated cells (37). The total decrease in CFTR-dependent Isc upon inhibition, denoted as ΔIsc_{inh172}, measures the effect of $CFTRinh_{172}$ in blocking the forskolin- and potentiator-stimulated current as well as the spontaneous constitutive CFTR current (37-39). The tracing in Figure 1A displays the short-circuit current (Isc) recorded from CF-HBE cells following 24-hour ETI treatment. Amiloride (apical, 100 μM) is used to inhibit the sodium current mediated by ENaC, followed by forskolin (apical, 1 μM), which stimulates Isc. This stimulation is subsequently reversed by the addition of $CFTRinh_{172}$ (apical, 10 μM), as depicted in the histogram on the right of Figure 1A. Lastly, UTP (apical, 100 μM) is added, eliciting the characteristic biphasic response of calcium-activated chloride channels, such as TMEM16a. As shown in Figure 1B, the effect of ETI is dependent on treatment duration. The traces presented compare CF-HBE cells treated with ETI for 4, 8, and 24 hours to cells without ETI treatment (DMSO-treated, left trace). Notably, the ENaC-dependent ΔIsc_{ami} gradually decreases from 16.7 ± 5 μA/cm² (no ETI) to 2.9 ± 0.5 μA/cm² (24-hour ETI, $p<0.05$) as measured by 2 technical replicates each from 2 unique donors, while the amplitude of F508del-CFTR currents (ΔIsc_{fsk}) increases from 0.5 ± 0.1 μA/cm² (no ETI) to 8.81 ± 0.7 μA/cm² (24-hour ETI, $p<0.05$) as measured by 2-3 technical replicates each from 2 unique donors. This aligns with the established interaction between CFTR and ENaC channels (40).

Then, we evaluated the impact of a 24-hour ETI treatment on Isc in CFBE41o- F508del-CFTR cells, comparing it with DMSO treatment (Figure S1B). The baseline Isc in ETI-treated cells was 12 ± 0.6 μA/cm² (n = 21), significantly higher than the 4 ± 0.6 μA/cm²

observed in DMSO-treated cells (n = 5, *p<0.0001*) (Figure S1B-C). This increase in spontaneous Isc demonstrates the activity of ivacaftor, which facilitates the opening of F508del-CFTR channels at the membrane, supported by the correctors elexacaftor and tezacaftor, as previously reported (37, 39, 41) (see also figure S1D). This effect is also illustrated in Figures 1B and 1C using CF-HBE cells, showing inhibition of Isc with $CFTRinh_{172}$. The forskolin-stimulated change in Isc (ΔIsc_{fsk}) in ETI-treated CFBE41o- F508del-CFTR cells was 32.4 ± 1.6 µA/cm² (n = 21), compared to 0.6 ± 0.08 µA/cm² in DMSO-treated cells (*p<0.0001*) (Figure S1B). Additionally, the $CFTRinh_{172}$-inhibited Isc in ETI-treated cells reached 36.5 ± 1.8 µA/cm² (n = 21), whereas DMSO-treated cells showed only 0.7 ± 0.12 µA/cm² (*p<0.0001*) (Figure S1B). Tezacaftor was used at a concentration of 18 µM (Figure S1B) as in (19). Lower concentrations of tezacaftor, combined with 3 µM elexacaftor and 1 µM ivacaftor, still provided concentration-dependent correction as shown figure S2.

Effect of the duration of ETI treatment on CFBE41o- F508del-CFTR properties

In the following experiments, CFBE41o- F508del-CFTR cells were treated with ET or ETI for 2, 4, 6, 8, or 24 hours and compared to the control (DMSO). We began by conducting a Western blot analysis to assess the C/(B+C) ratio, which reflects the amount of CFTR in its mature, complex-glycosylated C band form, to the total of CFTR proteins (mature and non-mature forms) relative to either DMSO-treated F508del CFBE41o- cells or WT-CFBE41o- cells (Figures 2A and S4). The maturation level of WT-CFTR proteins was 0.96 ± 0.03 (n = 5, Figures 2A). Notably, after 2 hours of ETI treatment in CFBE41o- F508del cells, we observed a greater presence of mature C forms compared to ET-treated cells (ETI: 0.32 ± 0.08, n = 5 vs. ET: 0.21 ± 0.07, n = 5). After 4 hours, the levels of mature C forms were similar between ETI- and ET-treated cells (non-significant). However, this trend reversed at 6, 8, and 24 hours, with ET-treated cells showing a higher quantity of mature CFTR at 24 hours (ET: 0.73 ± 0.07, n = 5 vs. ETI: 0.60 ± 0.05, n = 5). Although the maturation level did not reach that of WT-CFTR, the maximum amount of mature F508del-CFTR protein was detected after 24 hours of treatment with either ET or ETI (Figure 2A, B).

Next, we performed Ussing chamber experiments to assess the effect of treatment duration on Isc, as a measure of F508del-CFTR function. Isc was stimulated using 1 µM forskolin (empty triangle), followed by 1 µM ivacaftor (grey triangle), and finally inhibited with 10 µM $CFTRinh_{172}$ (black triangle) in cells treated for 2, 6, and 24 hours with ET (Figure 2C) or ETI (Figure 2D). Mean Isc activation values by forskolin /IVA and mean Isc inhibition

by $CFTR_{inh172}$ are shown figures 2E and 2F, respectively. For ET treatment, an initial correction phase was observed at 4 hours (23.39 ± 2 µA/cm² for 2 hours and 32.57 ± 5.9 µA/cm² for 4 hours), with a significant increase at 24 hours corresponding to chronic ivacaftor addition (43.07 ± 8.8 µA/cm², n = 3 *vs.* 24.13 ± 6.7 µA/cm², n = 3). In contrast, adding ivacaftor to ETI-treated cells did not produce an additional effect, unlike in ET-treated cells, as previously reported (37) and observed earlier (42). This lack of potentiation in ETI-treated cells may be due to the challenge of removing ivacaftor when used at micromolar concentrations (43).

Half-life of F508del-CFTR in ET- and ETI-treated cells

Capurro et al. estimated a half-life of approximately 6 hours for ET-corrected F508del-CFTR in CFBE41o- cells (44). To compare the turnover of F508del-CFTR after incubation with ET and ETI (Figures 3A and S5), we conducted two series of experiments using cycloheximide (CHX) to inhibit de novo protein synthesis at various time points (0, 1, 2, 4 hours). As anticipated, the mature C form of WT-CFTR proteins remained stable (Figures 3B), while the immature B form gradually decreased with longer CHX treatment (Figures 3B, C). The maturation of F508del-CFTR was analyzed in DMSO-, ET-, and ETI-treated CFBE41o- F508del-CFTR cells (Figure 3A). In both ET- and ETI-treated cells, the mature C and immature B forms of F508del-CFTR declined over time at various time points (0, 1, 2, 4 hours). Both treatments extended the half-life ($t_{1/2}$) of the mature C form of CFTR compared to DMSO. The presence of the potentiator ivacaftor slightly reduced this stabilizing effect on the mature C form ($t_{1/2}$ >4 hours for ET treatment versus approximately 3 hours for ETI). The $t_{1/2}$ of the immature B form was approximately 60 minutes for DMSO-treated F508del-CFTR and around 30-40 minutes for WT-CFTR and both ET- and ETI-treated F508del-CFTR (Figure 3C).

Additionally, we measured Isc in ETI-treated CFBE41o- F508del-CFTR cells incubated with CHX for different durations (0, 2, 4, 6, 8 hours, Figure 4A). In each experiment, Isc was stimulated with 1 µM forskolin (empty triangle) and inhibited with 10 µM $CFTR_{inh172}$ (black triangle). Isc_{fsk} decreased with longer CHX treatment. After just 2 hours of CHX treatment, both Isc_{fsk} and Isc_{inh172} were significantly reduced (Figure 4B, C). By 4 hours, the transepithelial current had decreased by more than 50%, aligning with our immunoblot findings that demonstrated a direct correlation between the level of mature C form of F508del-CFTR and the cAMP-dependent transepithelial Isc rescued by ETI (Figure 4D).

Effect of reducing concentrations of ETI on CFBE41o- F508del-CFTR maturation and function

In the next set of experiments, we assessed the impact of varying ETI concentrations on the maturation and function of F508del-CFTR. CFBE41o- F508del-CFTR cells were treated with ETI at reduced concentrations of 33%, 11%, 3.3%, and 1.1% of the full 100% ETI treatment (corresponding to 18 µM tezacaftor ; 3 µM elexacaftor ; 1 µM ivacaftor), alongside a DMSO control. Immunoblots (Figures 5 and S6) revealed that in cells treated with ETI at 3.3% and 1.1%, the mature C form of F508del-CFTR was very low compared to the 100% ETI treatment ($P < 0.0001$), rendering them indistinguishable from DMSO-treated controls (non significant), as confirmed by statistical analysis from four independent experiments (Figure 5). The level of the immature B form of F508del-CFTR remained constant regardless of treatment. Notably, even at 11% of the full ETI treatment, the C/(B+C) ratio shows that the mature C form of F508del-CFTR was 50-60% compared to the 100% ETI control (Figure 5). Additionally, there was no significant difference in the mature C form level between cells treated with 100% and 33% ETI (Figure 5).

We then measured Isc in CFBE41o- F508del-CFTR cells after 24-hour incubation with ETI at the same concentration gradients. As in previous experiments, Isc was stimulated with forskolin (1 µM, empty triangle) and inhibited with $CFTRinh_{172}$ (10 µM, black triangle). At 33% of the full ETI concentration, the change in current was comparable to that observed with 100% ETI treatment (Figure 6). However, at 11%, ΔIsc_{fsk} was significantly reduced, with a mean value of 14.5 µA/cm² (Figures 6A, B). This reduction continued at 1.1% ETI concentration (ΔIsc_{fsk} = 4.74 µA/cm²), though it remained significantly higher than the DMSO control (ΔIsc_{fsk} = 1.19 µA/cm²). Quantification of ΔIsc_{inh172} revealed parallel changes in current for both activating and inhibitory phases (Figure 6C). Ivacaftor's ability to activate CFTR constitutively, as demonstrated here and in prior studies (37, 39, 41), was confirmed by quantification of pre-activation Isc levels, showing probable dependence on ivacaftor concentration (Figure 6D).

Whole-cell patch clamp recordings of wild-type and F508del-CFTR chloride currents in CFBE41o- cells

We conducted whole-cell patch-clamp experiments (Figure 7) using CFBE41o- cells expressing either WT-CFTR or F508del-CFTR, treated for 24 hours with ETI or DMSO as a

control. As anticipated, whole-cell recordings for WT-CFTR demonstrated a linear relationship between Cl^- currents and voltage, with a significant increase in conductance upon stimulation with forskolin (fsk) and genistein (gst) compared to baseline (mean current density at +40 mV, $I_{fsk/gst}$ = 336 ± 32.94 pA/pF, n = 25; upper traces in figure 7A and corresponding current density curves in figure 7B-D). For CFBE41o- F508del-CFTR cells, negligible Cl^- current was detected under DMSO conditions (middle traces in figure 7A and current density curves in figure 7C, $I_{fsk/gst}$ = 3.2 ± 0.8 pA/pF, n = 6). When cells were treated with ETI for 24 hours, the recorded CFTR current was 211 ± 33.75 pA/pF at +40 mV (n = 10; lower traces in figure 7A and current density curves in figure 7D), corresponding to approximately 63% of the current recorded in CFBE41o- WT-CFTR cells (p<0.05, Figure 7B, E).

Next, we examined whole-cell currents in CFBE41o- F508del-CFTR cells treated with ETI at 33%, 11%, 3.3%, and 1.1% concentrations (Figure 7D, E). Similar to our Ussing chamber results, the patch-clamp data indicated that reducing ETI concentration to 33% still supported a significant fsk/gst-dependent F508del-CFTR current ($I_{fsk/gst}$ = 204 ± 42.3 pA/pF, n = 14), comparable to that observed with 100% ETI. Further reductions in ETI concentration resulted in progressively lower current densities at +40 mV ($I_{fsk/gst}$ = 130 ± 15.9 pA/pF for ETI 11%, n = 23; $I_{fsk/gst}$ = 87 ± 22 pA/pF for ETI 3.3%, n = 11; and $I_{fsk/gst}$ = 3.22 ± 0.8 pA/pF for ETI 1.1%, n = 6). At 11% ETI, the rescued F508del-CFTR-dependent chloride current amplitude was approximately 60% of that observed with 100% ETI, consistent with our immunoblot analysis (Figure 5) showing a mature C form of F508del-CFTR at around 60% of the level quantified with 100% ETI.

Significant increase in temperature stability of F508del-CFTR-dependent Isc by ETI

In addition to abnormal maturation and function, F508del-CFTR also demonstrates thermal instability at physiological temperatures, even following correction with VX809 or exposure to low temperatures (12-15). Since no data currently exist regarding the effect of ETI on this defect, we treated CF-HBE cells (Figures 8A, C) and CFBE41o- F508del-CFTR cells (Figures 8B, C) with ETI for 24 hours. Once activated by forskolin, we recorded Isc for 60 to 120 minutes at a controlled temperature of 37 ± 1°C. $CFTRinh_{172}$ was added to the apical chamber at the end of the experiment to inhibit the remaining CFTR-dependent Isc.

For CFBE41o- WT-CFTR cells, Isc_{fsk} was stable and, in some cases, even increased over time (Figure 8B, dotted line; quantified in Figure 8C). In contrast, in ETI-treated CF-HBE and CFBE41o- F508del-CFTR cells, the current gradually declined over time. Figure 8B

shows recordings of fsk-activated F508del-CFTR Isc with corresponding $CFTRinh_{172}$ inhibition after 10 to 80 minutes. Notably, F508del-CFTR Isc remained stable for approximately the first 10 minutes before gradually and spontaneously decreasing. By 120 minutes, the fsk-activated ETI-rescued F508del-CFTR Isc had decreased by approximately 90% (Figure 8C). Interestingly, in ETI-treated CFBE41o- F508del-CFTR cells, likely due to the constitutive pool of F508del-CFTR channels already rescued and activated by ivacaftor, the $CFTRinh_{172}$-dependent F508del-CFTR Isc still accounted for about 50% of the total F508del-CFTR current (Figure 8C). These findings indicate that after two hours, approximately half of the ETI-corrected F508del-CFTR-dependent transepithelial current remained present, an outcome not observed without ETI treatment (15).

Effect of bamocaftor on F508del-CFTR-dependent Isc

Bamocaftor (VX-659, chemical structure shown at the bottom of Figure 9) was evaluated in clinical studies for pwCF alongside elexacaftor (27). Interestingly, the airway inflammatory milieu from late- and early-stage CF lung disease improves the efficacy of CFTR modulators, regardless of the combination therapy used with ETI or BTI (45). Here, we assessed the effects of bamocaftor on various aspects of F508del-CFTR function, including its maturation and thermal stability. Bamocaftor (3 μM) was combined with tezacaftor (3 μM) and ivacaftor (1 μM) to form a preparation referred to as BTI. This combination was compared to ETI at the same concentrations and to a third preparation consisting of bamocaftor, elexacaftor, and ivacaftor, referred to as BEI in Figures 9A and 9B. The triple BTI combination was significantly more effective than either ETI or BEI (Figure 9B). Bamocaftor, like elexacaftor (28, 42), rescues F508del-CFTR in synergy with tezacaftor (Figure S3). After adding forskolin and VX770, the ΔIsc_{inh172} was 4.8 ± 1.2 μA/cm², 27 ± 0.75 μA/cm² and 81 ± 5.6 μA/cm² for Tezacaftor-, Bamocaftor-, and Tezacaftor/Bamocaftor - treated CFBE41o- F508del-CFTR cells, respectively (n=3-6).

As for ETI-corrected cells, we analyzed the maturation of F508del-CFTR proteins in DMSO- and BTI-treated CFBE41o- F508del-CFTR cells. The mature C form of F508del-CFTR was robustly and significantly increased by BTI treatment compared to DMSO (Figures 9D and S7). We also studied the effect of reducing BTI concentrations (defined as 100%, corresponding to 3 μM bamocaftor, 3 μM tezacaftor, and 1 μM ivacaftor) to 50% (1.5 μM bamocaftor, 1.5 μM tezacaftor, and 0.5 μM ivacaftor) and 10% (0.3 μM bamocaftor, 0.3 μM tezacaftor, and 0.1 μM ivacaftor) on both function (Figure 9C) and maturation (Figures 9D, E). The rescue of the band C form was already apparent at 10% BTI concentration

compared to DMSO and further increased at 50% and 100%, with no significant difference observed between the latter two conditions under full BTI treatment (Figure 9E).

Finally, we compared the effect of BTI and ETI on the thermal stability of F508del-CFTR following forskolin stimulation. Interestingly, Figure 10A shows that although the Isc in BTI-treated cells continues to decline over time, the remaining current amplitude after 2 hours is significantly higher than in ETI-treated cells ($p<0.001$). Quantitative analysis of multiple experiments is presented in Figure 10B. After 120 minutes, the forskolin-activated BTI-rescued F508del-CFTR Isc had decreased by approximately 75%, while the $CFTR_{inh172}$-dependent BTI-rescued F508del-CFTR Isc still accounted for about 60% of the total F508del-CFTR-dependnet Isc (Figure 10B).

DISCUSSION

Our study demonstrates that the impact of highly effective CFTR modulator therapy (HEMT) treatment is influenced by the treatment duration, as well as the maturation, turnover, and thermal stability of F508del-CFTR currents at physiological temperature. Notably, short-term treatment (2-4 hours) was insufficient to reveal the destabilizing effect of ivacaftor on F508del-CFTR, whereas long-term treatment promoted destabilization, consistent with prior reports (35-37). Chronic ETI treatment extended the half-life of corrected F508del-CFTR from 45 minutes to 180 minutes (a fourfold increase), and this stabilization was further enhanced when ivacaftor was omitted (ET treatment), resulting in a half-life exceeding 4 hours, underscoring ivacaftor's destabilizing effect.

Our findings also revealed that the correction efficacy of F508del-CFTR by ETI/BTI is dose-dependent and contingent on the precise ratio of its components. We observed a progressive decline in functional correction as the ETI concentration decreased from 10% to 1% of the initial dose. However, reducing the dose at 33% of the standard ETI concentration maintained correction levels comparable to 100% ETI. This observation aligns with the clinical variability in recommended ETI doses for pwCF, which differ based on age and weight. For individuals over 6 years old, the ETI dose is two tablets of 50/25/37.5 mg for patients under 30 kg, and double that for those over 30 kg. For younger children (ages 2-5), the dose is one tablet of either 80/40/60 mg or 100/50/75 mg, depending on whether they weigh under or over 14 kg, with an additional ivacaftor tablet (59.5, 75, or 150 mg) taken 12 hours later.

Although *in vitro* ETI concentrations cannot be directly extrapolated to *in vivo* dosing, understanding the impact of reduced ETI doses is crucial in the context of potential adverse effects (AEs), such as hepatotoxicity (46, 47), and drug interactions involving ETI components (47, 48). Recent physiologically-based pharmacokinetic (PBPK) modeling indicates that lower ETI doses (e.g., half-doses, alternate-day dosing, or thrice-weekly administration) can be effective for pwCF experiencing adverse effects (46, 48). Notably, reduced ETI dosing has been linked to improve mental health outcomes without significant clinical deterioration (48, 49). Hong et al.'s modeling predicted mean trough concentrations of 0.89, 0.83, and 0.79 mg/L for reduced ETI dosing, while the lowest therapeutic dose of elexacaftor (50 mg daily) yielded a trough concentration of 0.49 mg/L. Our data indicate that this range, equivalent to 33%-11% of the full ETI dose, is sufficient to achieve 60%-100% efficacy. Additionally, PBPK simulations (50) demonstrated that lung concentrations of elexacaftor and ivacaftor, even at reduced daily doses (50-200 mg for elexacaftor and 25-150 mg for ivacaftor), exceeded their EC_{50} values. Only tezacaftor at the lowest tested dose (10 mg daily) fell below its EC_{50} value, suggesting that efficacy could be maintained even with dose reduction, also supported by our *in vitro* findings.

A notable aspect of our study is the documented thermal instability of F508del-CFTR at physiological temperature (37±1°C), where channel activity rapidly declines within 15 minutes. This instability persists despite low-temperature cell culture (27°C) or treatment with the type I corrector VX-809 (Lumacaftor) (12-15). Our results extend this understanding by showing that even the highly effective ETI or BTI combinations only partially address this defect. The apparently greater effect of bamocaftor compared to elexacaftor is likely due to a higher fsk peak BTI (see Fig. 10). The decline follows a similar pattern to that of ETI, but since it starts from a higher Isc value, it takes a longer time to decline. Thus, with either bamocaftor or elexacaftor, the thermal instability at 37°C appears comparable. This raises critical questions about the optimal duration of F508del-CFTR activity at the plasma membrane during therapy.

The complex role of ivacaftor also warrants attention due to reports of "ivacaftor withdrawal syndrome," characterized by rapid respiratory symptom onset and a significant (>20%) decline in FEV1 following discontinuation (51, 52). Similarly, acute exacerbations and lung function declines have been noted after ETI discontinuation (53). Our study, shows that (i) short-term ETI treatment does not trigger ivacaftor's destabilizing effect, (ii) ETI slows turnover by a factor of four compared to DMSO, (iii) at 33% ETI, correction remains

comparable to 100% ETI, and (iv) the thermal stability of F508del-CFTR at physiological temperature is notably superior to that observed with lumacaftor/ivacaftor (12, 13, 15) or tezacaftor/ivacaftor (unpublished data).

In conclusion, our *in vitro* findings indicate that reduced doses of HEMT can effectively sustain therapeutic efficacy, underscoring the potential of dose optimization strategies to minimize side effects in pwCF. One limitation of our study is that it included only human bronchial epithelial cells from female patients. Although initially promising, bamocaftor did not demonstrate sufficient benefits to justify its continued development as a therapy for cystic fibrosis. Its therapeutic development was discontinued in favor of the combination involving elexacaftor (www.cff.org). The combination of elexacaftor, tezacaftor, and ivacaftor has taken its place, providing a significant advancement for patients with this disease. Looking ahead, we anticipate that future therapies - whether leveraging current correctors or introducing novel compounds - will further improve the stability and function of F508del-CFTR at physiological temperatures, either as standalone options or in combination with ETI or new correctors.

ETHICAL APPROVAL

Human tissues from F508del/F508del donors were collected and used according to the French law, with the informed consent of patients and through the authorization of Biological Collection n°DC-2012-1583 obtained from the French Ministry of Higher Education and Research, and with the approval n°21-775 of IRB 00003888.

DATA AVAILABILITY

The datasets generated during and/or analysed during the current study are available from the corresponding author on reasonable request.

SUPPLEMENTAL MATERIAL

Supplemental material available at https://doi.org/10.6084/m9.figshare.29402219

Figure S1. Effect of ETI on Isc in CFBE41o-F508del-CFTR cells.

Figure S2. Effect of various concentration of tezacaftor on Isc in CFBE41o-F508del-CFTR cells in the presence of fixed concentrations of elexacaftor and invacaftor.

Figure S3. Synergy between bamocaftor and tezacaftor in CFBE41o- F508del-CFTR cells.

Figures S4 to S7. Uncropped images of western blot experiments

GRANTS

This study was supported by Vaincre La Mucoviscidose (RF20200502704) and ManRos Therapeutics. TC hold a thesis scholarship from ManRos Therapeutics and ANRT (CIFRE).

DISCLOSURES

TC doctoral fellowship was supported by ManRos Therapeutics and ANRT (CIFRE).

Other authors declare that they have no conflict of interest.

AUTHOR CONTRIBUTIONS

TC, SM and CB did cell cultures. TC and SM performed and analyzed Western blot experiments. TC, SM, FD and FB performed and analyzed data of Ussing chamber. TC and FB performed and analyzed data of patch clamp experiments. TC, CV and FB wrote and edited the manuscript. FB designed the experiments and contributed reagents/materials/analysis tools.

ACKNOWLEDGMENTS

We thank Prof Edouard Sage and Dr. Christelle Coraux for providing human airway epithelial samples, Dr. Laurent Meijer for discussion, advise and support. Authors also thank Isabelle Fixe for technical assistance.

REFERENCES

1. Riordan JR, Rommens JM, Kerem B, et al. Identification of the cystic fibrosis gene: cloning and characterization of complementary DNA. Science. 1989; 245:1066–1073.

2. Rommens JM, Iannuzzi MC, Kerem B, et al. Identification of the cystic fibrosis gene: chromosome walking and jumping. Science. 1989; 245:1059–1065.

3. Kerem B, Rommens JM, Buchanan JA, et al. Identification of the cystic fibrosis gene: genetic analysis. Science. 1989; 245:1073–1080.

4. Shteinberg M, Haq IJ, Polineni D, Davies JC. Cystic fibrosis. Lancet 397, 2195–2211 (2021). [PubMed: 34090606].

5. Lakli M, Onnée M, Carrez T, Becq F, Falguières T, Fanen P. ABC transporters involved in respiratory and cholestatic diseases: From rare to very rare monogenic diseases. Biochem Pharmacol. 2024 Aug 5;229:116468. doi: 10.1016/j.bcp.2024.116468.

6. Zhang Z, Chen J, Atomic Structure of the Cystic Fibrosis Transmembrane Conductance Regulator. Cell 167, 1586–1597 e1589 (2016). [PubMed: 27912062].

7. Saint-Criq V, Gray MJ. Role of CFTR in epithelial physiology. Cellular and Molecular Life Sciences, 2017, 74 (1), pp.93-115. 10.1007/s00018-016-2391-y.

8. Cheng SH, Gregory RJ, Marshall J, Paul S, Souza DW, White GA, et al. Defective intracellular transport and processing of CFTR is the molecular basis of most cystic fibrosis. Cell 1990; 63: 827–834.

9. Dalemans W, Barbry P, Champigny G, Jallat S, Dott K, Dreyer D, et al. Altered chloride ion channel kinetics associated with the delta F508 cystic fibrosis mutation. Nature 1991; 354: 526–528.

10. Lukacs GL, Chang XB, Bear C, Kartner N, Mohamed A, Riordan JR, et al. The delta F508 mutation decreases the stability of cystic fibrosis transmembrane conductance regulator in the plasma membrane. Determination of functional half-lives on transfected cells. J. Biol. Chem. 1993; 268: 21592–8.

11. Wang W, Okeyo GO, Tao B, Hong JS, Kirk KL. Thermally Unstable Gating of the Most Common Cystic Fibrosis Mutant Channel (ΔF508): "Rescue" by Suppressor Mutations in Nucleotide Binding Domain 1 and by Constitutive Mutations in the Cytosolic Loops. J. Biol. Chem. 2011; 286: 41937–41948.

12. Boinot, C., Jollivet Souchet, M., Ferru-Clement, R. & Becq, F. Searching for Combinations of Small-Molecule Correctors to Restore F508del-Cystic Fibrosis Transmembrane Conductance Regulator Function and Processing. J. Pharmacol. Exp. Ther. 2014; 350, 624–634.

13. Billet, A., Froux, L., Hanrahan, J. W. & Becq, F. Development of Automated Patch Clamp Technique to Investigate CFTR Chloride Channel Function. Front. Pharmacol. 8, (2017) Apr 7:8:195.

14. Meng, X. et al. Two Small Molecules Restore Stability to a Subpopulation of the Cystic Fibrosis Transmembrane Conductance Regulator with the Predominant Disease-causing Mutation. J. Biol. Chem. 2017; 292, 3706–3719.

15. Froux L, Coraux C, Sage E, Becq F. The Short-term consequences of F508del-CFTR thermal instability on CFTR-dependent transepithelial currents in human airway epithelial cells. Scientific Report. 2019 Sep 24;9(1):13729. doi: 10.1038/s41598-019-50066-7.

16. Okiyoneda T, Veit G, Dekkers JF, Bagdany M, Soya N, Xu H, et al. Mechanism-based corrector combination restores ΔF508-CFTR folding and function. Nat. Chem. Biol. 2013; 9, 444–454.

17. Froux L, Billet A, Becq F. Modulating the cystic fibrosis transmembrane regulator and the development of new precision drugs. Expert Rev. Precision Med and Drug Dev. 2018, 3, 357-370. DOI: 10.1080/23808993.2018.1547109

18. Yeh HI, Sutcliffe KJ, Sheppard DN, Hwang TC. CFTR Modulators: From Mechanism to Targeted Therapeutics. Handb Exp Pharmacol. 2022 Aug 17. doi: 10.1007/164_2022_597. Online ahead of print. PMID: 35972584

19. Keating D, Marigowda G, Burr L, Daines C, Mall MA, McKone EF, et al. VX-445-Tezacaftor-Ivacaftor in Patients with Cystic Fibrosis and One or Two Phe508del Alleles. N Engl J Med. 2018; 379(17): 1612-1620.

20. Heijerman HGM, McKone EF, Downey DG, Van Braeckel E, Rowe SM, Tullis E, et al. Efficacy and safety of the elexacaftor plus tezacaftor plus ivacaftor combination regimen in

people with cystic fibrosis homozygous for the F508del mutation: a double-blind, randomised, phase 3 trial. Lancet. 2019; 394(10212): 1940-1948.

21. Middleton PG, Mall MA, Drevinek P, et al. Elexacaftor-tezacaftor-ivacaftor for cystic fibrosis with a single phe508del allele. N Engl J Med. 2019; 381(19): 1809-1819.

22. Van Goor F, Hadida S, Grootenhuis PD, Burton B, Cao D, Neuberger T, Turnbull A, Singh A, Joubran J, Hazlewood A, et al. Rescue of CF airway epithelial cell function in vitro by a CFTR potentiator, VX-770. Proc Natl Acad Sci USA 2009; 106: 18825–30.

23. Liu F, Zhang Z, Levit A, Levring J, Touhara KK, Shoichet BK, Chen J. Structural identification of a hotspot on CFTR for potentiation Science. 2019 June 21; 364(6446): 1184–1188. doi:10.1126/science.aaw7611.

24. Laselva O, Bartlett C, Gunawardena TNA, Ouyang H, Eckford PDW, Moraes TJ, Bear CE and Gonska T. Rescue of multiple class II CFTR mutations by elexacaftor+tezacaftor+ivacaftor mediated in part by the dual activities of elexacaftor as both corrector and potentiator Eur Respir J. 2021a Jun; 57(6): 2002774. doi: 10.1183/13993003.02774-2020.

25. Veit, G., C. Vaccarin, and G.L. Lukacs, Elexacaftor co-potentiates the activity of F508del and gating mutants of CFTR. J Cyst Fibros, 2021. 20(5): p. 895-898.

26. Shaughnessy, C.A., P.L. Zeitlin, and P.E. Bratcher, Elexacaftor is a CFTR potentiator and acts synergistically with ivacaftor during acute and chronic treatment. Sci Rep, 2021. 11(1): p. 19810.

27. Davies JC, Moskowitz SM, Brown C, Horsley A, Mall MA, McKone EF, Plant BJ, Prais D, Ramsey BW, Taylor-Cousar JL, Tullis E, Uluer A, McKee CM, Robertson S, Shilling RA, Simard C, Van Goor F, Waltz D, Xuan F, Young T, Rowe SM; VX16-659-101 Study Group. VX-659-Tezacaftor-Ivacaftor in Patients with Cystic Fibrosis and One or Two Phe508del Alleles. N Engl J Med. 2018 Oct 25;379(17):1599-1611. doi: 10.1056/NEJMoa1807119. Epub 2018 Oct 18. PMID: 30334693

28. Fiedorczuk K, Chen J. Molecular Structures Reveal Synergistic Rescue of Δ508 CFTR by Trikafta Modulators Science. 2022a October 21; 378(6617): 284–290.

29. Ren HY, Grove DE, De La Rosa O, Houck SA, Sopha P, Van Goor F, et al. VX-809 corrects folding defects in cystic fibrosis transmembrane conductance regulator protein through action on membrane-spanning domain 1. Gilmore R, editor. Mol Biol Cell. 2013 Oct;24(19):3016–24.

30. Loo TW, Clarke DM. Corrector VX-809 promotes interactions between cytoplasmic loop one and the first nucleotide-binding domain of CFTR. Biochem Pharmacol. 2017 Jul 15;136:24–31.

32. Laselva O, Molinski S, Casavola V, Bear CE. Correctors of the major cystic fibrosis mutant interact through membrane-spanning domains. Molecular Pharmacology June 2018, 93 (6) 612-618.

33. Fiedorczuk K, Chen J, Mechanism of CFTR correction by type I folding correctors. Cell 2022b, 185, 158–168 e111. [PubMed: 34995514].

34. Laselva O, Qureshi Z, Zeng ZW, Petrotchenko EV, Ramjeesingh M, Hamilton CM, Huan L-J, Borchers CH, Pomes R, Young R, Bear CE. Identification of binding sites for ivacaftor

650 on the cystic fibrosis transmembrane conductance regulator. iScience 2021b; 24, 102542,
651 June 25.

652 35. Cholon DM, Quinney NL, Fulcher ML, Esther CR, Das J, Dokholyan NV, Randell SH,
653 Boucher RC, Gentzsch M. Potentiator ivacaftor abrogates pharmacological correction of
654 ΔF508 CFTR in cystic fibrosis. Sci. Transl. Med. 2014; 6: 246ra96.

655 36. Veit G, Avramescu RG, Perdomo D, et al. Some gating potentiators, including VX-770,
656 diminish ΔF508-CFTR functional expression. Sci Transl Med. 2014; 6(246): 246ra97.

657 37. Becq F, Mirval S, Carrez T, et al. The rescue of F508del-CFTR by
658 elexacaftor/tezacaftor/ivacaftor (Trikafta) in human airway epithelial cells is underestimated
659 due to the presence of ivacaftor. Eur Respir J. 2022;59(2):2100671.

660 38. Ma T, Thiagarajah JR, Yang H, Sonawane ND, Folli C, Galietta LJV, et al.
661 Thiazolidinone CFTR inhibitor identified by high-throughput screening blocks cholera toxin –
662 induced intestinal fluid secretion. J. Clin. Invest. 2002; 110: 1651–1658.

663 39. Shaughnessy CA, Zeitlin PL, Bratcher PE. Net benefit of ivacaftor during prolonged
664 tezacaftor/elexacaftor exposure in vitro. J Cyst Fibros. 2022 Jul;21(4):637-643.
665 doi:10.1016/j.jcf.2022.02.011. Epub 2022 Mar 2

666 40. Stutts MJ, Canessa CM, Olsen JC, Hamrick M, Cohn JA, Rossier BC, Boucher RC. CFTR
667 as a cAMP-dependent regulator of sodium channels. Science 1995;269:847–850. [PubMed:
668 7543698]

669 41. Nick HJ, Christeson SE, Bratcher PE. The Functional Impact of VX-770 on the Cystic
670 Fibrosis Transmembrane Conductance Regulator Is Enduring and Increases the Constitutive
671 Activity of This Channel in Primary Airway Epithelia Generated from Healthy Donors.
672 Biomolecules. 2024 Oct 29;14(11):1378. doi: 10.3390/biom14111378.

673 42. Veit G, Roldan A, Hancock MA, Da Fonte DF, Xu H, Hussein M, et al. Allosteric folding
674 correction of F508del and rare CFTR mutants by elexacaftor-tezacaftor-ivacaftor (Trikafta)
675 combination. JCI Insight. 2020;5(18): e139983.

676 43. Csanády, L. and B. Törőcsik, Cystic fibrosis drug ivacaftor stimulates CFTR channels at
677 picomolar concentrations. eLife, 2019. 8: p. e46450.

678 44. Capurro V, Tomati V, Sondo E, Renda M, Borrelli A, Pastorino C, Guidone D, Venturini
679 A, Giraudo A, Bertozzi SM, Musante I, Bertozzi F, Bandiera T, Zara F, Galietta LJV,
680 Pedemonte N. Partial rescue of F508del-CFTR stability and trafficking defects by double
681 corrector treatment. Int. J. Mol. Sci. 2021, 22, 5262

682 45. Gentzsch M, Cholon DM, Quinney NL, Martino MEB, Minges JT, Boyles SE, Guhr Lee
683 TN, Esther CR Jr, Ribeiro CMP. Airway Epithelial Inflammation In Vitro Augments the
684 Rescue of Mutant CFTR by Current CFTR Modulator Therapies. Front Pharmacol. 2021 Mar
685 30;12:628722. doi: 10.3389/fphar.2021.628722. eCollection 2021. PMID: 33859562

686 46. Dagenais RVE , Su VCH, Quon BS. Real-world safety of CFTR modulators in the
687 treatment of cystic fibrosis: A Systematic Review. J. Clin. Med. 2021, 10, 23.

688 47. Purkayastha D, Agtarap K, Wong K, Co J, Pakhale S, Kanji S. Drug-drug interactions
689 with CFTR modulator therapy in cystic fibrosis: Focus on Trikafta®/Kaftrio®. Journal of
690 Cystic Fibrosis. Volume 22, Issue 3, May 2023, Pages 478-483.

48. Hong E, Shi A, Beringer P. Drug-drug interactions involving CFTR modulators: a review of the evidence and clinical implications. Expert Opin Drug Metab Toxicol. 2023a Apr;19(4):203-216. doi: 10.1080/17425255.2023.2220960. Epub 2023 Jun 6.

49. Spoletini G, Gillgrass L, Pollard K, Shaw N, Williams E, Etherington C, Clifton IJ, Peckham DG. Dose adjustments of Elexacaftor/Tezacaftor/Ivacaftor in response to mental health side effects in adults with cystic fibrosis. J Cyst Fibros. 2022 Nov;21(6):1061-1065. doi: 10.1016/j.jcf.2022.05.001.

50. Hong E, Li R, Shi A, Almond LM, Wang J, Khudari AZ, Haddad S, Sislyan S, Angelich M, Chung PS , Rao AP, Beringer PM. Safety of elexacaftor/tezacaftor/ivacaftor dose reduction: Mechanistic exploration through physiologically based pharmacokinetic modeling and a clinical case series. Pharmacotherapy. 2023b Apr;43(4):291-299. doi: 10.1002/phar.2786.

51. Trimble AT, Donaldson SH. Ivacaftor withdrawal syndrome in cystic fibrosis patients with the G551D mutation. J Cyst Fibros 2018;17(2):e13–e6.

52. Clegg JM, Malloy KW, Brown RF, Grisso AG, Sokolow AG. Ivacaftor withdrawal syndrome: a potentially life-threatening consequence from a life-saving medication. J Cyst Fibros 2022 May;21(3):549-550. doi: 10.1016/j.jcf.2021.07.021. Epub 2021 Aug 11.

53. Mitropoulou G, Balmpouzis Z, Plojoux J, Dotta-Celio J, Sauty A, Koutsokera A. Effects of elexacaftor-tezacaftor-ivacaftor discontinuation in cystic fibrosis. Respir Med Res. 2022;82:100972. doi:10.1016/j.resmer.2022.100972

FIGURE LEGENDS

Figure 1. Recordings of Isc in ETI - human F508del-CFTR bronchial epithelial cells. (A) Representative short circuit current (Isc) recording of a ALI culture of F508del/F508del human bronchial epithelial cells (CF-HBE cells) treated by ETI. We first added apical amiloride (noted Ami, black triangle) to inhibit ENaC-dependent sodium current and then forskolin (noted Fsk, empty triangle) to activate the ETI corrected-F508del-CFTR current. Isc was inhibited by $CFTR_{inh172}$ (noted Inh172, second black triangle) and UTP (noted UTP, second empty triangle) was added at the end of the recording to activate calcium-dependent chloride secretion. On the right is shown quantification of the corresponding Isc activated by fsk (black squares) calculated from the peak Isc response minus the basal activity (ΔIsc) and Isc inhibited by $CFTR_{inh172}$ measured by the difference between the plateau after fsk activation and the current after $CFTR_{inh72}$ application (empty squares). Number of experiments: 2-3 technical replicates each from 3 unique donors. Concentrations used are: 100 µM amiloride, 1 µM fsk, 10 µM $CFTR_{inh172}$ and 100 µM UTP. (B) example recordings of ALI cultures of CF-HBE cells from a F508del-CFTR patient treated 4h, 8h and 24h by ETI compared to control CF-HBE cells (cells only treated with DMSO). Concentrations used are: amiloride

729 (100 µM, black triangle), fsk (1 µM, empty triangle) and $CFTR_{inh172}$ (10 µM, black triangle),
730 as indicated on each trace. ETI: 18 µM tezacaftor ; 3 µM elexacaftor; 1 µM ivacaftor.
731
732 **Figure 2: Effect of the duration of ETI and ET treatments on F508del-CFTR proteins.**
733 (A) Immuno-blot detection of F508del-CFTR in whole lysates derived from CFBE41o-
734 F508del-CFTR cells with vehicle (DMSO) and correctors (18 µM tezacaftor ; 3 µM
735 elexacaftor) with or without 1 µM ivacaftor (as indicated by the + symbols) at different time
736 points (2, 4, 6, 8 and 24h). (B) Corresponding quantification of the ratio of mature CFTR
737 proteins on total (C/(B+C)). Data are expressed as mean ± (n=5 for all experimental
738 conditions). The data are compared to DMSO treatment. For WT (right bar), the data are
739 compared to the ETI 24h condition. (C, D) Representative tracings of Isc as function of time
740 for CFBE41o-F508del-CFTR cells incubated at different time with ET (C) and ETI (D)
741 treatments. Isc is stimulated by fsk (1 µM, empty triangle) and ivacaftor (1 µM, grey triangle)
742 and inhibited by $CFTR_{inh172}$ (10 µM, black triangle). (E, F) Corresponding quantification of
743 CFTR activation by fsk/IVA (E) and inhibition by $CFTR_{inh172}$ (F). Data are expressed as mean
744 ± SD (n=3 for all experimental conditions). Data compared to DMSO; ****$p<0.0001$.
745

Figure 3: Effect of CHX treatments on ETI-corrected without (ET) and with potentiator (ETI) on F508del-CFTR half-time (A, B) Immuno-blot detection of CFTR in whole lysates from F508del-CFTR (A) and wild-type (B) expressing CFBE41o- cells treated with vehicle (DMSO), correctors (18 μM tezacaftor, 3 μM elexacaftor) with or without 1 μM ivacaftor, at different time points following CHX induced block of protein synthesis. (C) Quantification of F508del-CFTR and WT (band C and B) half time normalized by the value at time =0. Data are expressed as mean ± SD (n=4 for all except WT n=5).

Figure 4: Effect of CHX treatment on Isc with ETI-corrected without (ET) and with potentiator (ETI) CFBE41o- F508del-CFTR cells. (A) Original tracings of Isc as function of time for CFBE41o-F508del-CFTR cells incubated 24h with ETI treatments and at different time points following CHX induced block of protein synthesis. (B, C) Corresponding quantification of CFTR current activation by fsk (1 μM, B) and inhibition by $CFTR_{inh172}$ (10 μM, C). (D) plot of the Δfsk-activated Isc (from panel B) versus band C intensity (data from Fig.3) showing a linear relationship as function of CHX treatment duration. Data are expressed as mean ± SD (n=3-9). Statistics are versus control ETI (0 CHX); ****: $p<0.0001$.

Figure 5. Immunoblots with different concentrations of ETI on CFBE41o- F508del-CFTR protein. Immuno-blot detection CFTR in whole lysates derived from F508del-CFTR treated with vehicle (DMSO); correctors + potentiator (18 μM tezacaftor; 3 μM elexacaftor + 1 μM ivacaftor) with decreasing concentrations 33%, 11%, 3.3 and 1.1% ETI. Our loading control is GAPDH (bottom line). Corresponding quantification of F508del-CFTR band C/(B+C) ratio. Data are expressed as mean ± SD (n=4 for all conditions) compared to DMSO or between two ETI concentrations as indicated by the horizontal bar; ****$p<0.0001$.

Figure 6. Effect of different concentrations of ETI on Isc in CFBE41o- F508del-CFTR protein. (A) Original tracings of Isc CFTR activation by fsk (1μM, empty triangle) and inhibition by $CFTR_{inh172}$ (10 μM, black triangle) for CFBE41o-F508del-CFTR cells incubated 24h with decreasing concentrations 33%, 11%, 3.3%, 1.1% ETI or DMSO. (B-D) Corresponding quantification of CFTR activation by fsk (B), inhibition by $CFTR_{inh172}$ (C), and pre-activation (between basal and inhibition, D). Data are expressed as mean ± SD (n=3-5) compared to ETI 100% or between two ETI concentrations as indicated by the horizontal bar; ****$p<0.0001$.

Figure 7. Whole-cell patch clamp recordings of wild-type and F508del-CFTR chloride current in CFBE41o- cells at decreasing concentration of ETI. (A) Exemplar currents traces of WT and F508del-CFTR recorded in F508del-CFTR expressing CFBE41o- cells as indicated on the right. F508del-CFTR cells were treated with DMSO or ETI. Left traces show the basal chloride currents; middle traces the chloride current activated by fsk+gst (10 μM; 30 μM) and on the right the chloride current after adding in the bath 10 μM $CFTR_{inh172}$. (B-D) Current density/Voltage relationships from wild-type (B) and F508del-CFTR (C, D) expressing CFBE41o- cells treated with the vehicle DMSO (C), treated cells by ETI, correctors (18 μM tezacaftor ; 3 μM elexacaftor) + 1 μM ivacaftor (D), at different concentration of ETI as indicated on each graph. Activation by Fsk+Gst (empty squares), inhibition by $CFTR_{inh172}$ (filled squares) and in basal condition (empty circles). (E) Corresponding quantification of current densities recorded at +40mV in the presence of Fsk+Gst. Data are expressed as mean ± SD (n=3-25). Data compared to DMSO; $^{****}p<0.0001$.

Figure 8. Functional thermal instability of CFTR-dependent Isc. (A) two representative tracings of Isc from two different donors for F508del-CFTR HBE cells recorded during 90 min at 37°C as indicated above tracings. (B) Original tracings of Isc with WT and F508del-CFBE41o- cells recorded during 80-120 min at 37°C as indicated above tracings. Isc was activated by fsk (1 μM) and inhibited 80-120 min later by $CFTR_{inh172}$ (10 μM). Cells were treated with ETI (indicated for each tracing), except in (B) for WT-CFBE41o- cells. Original lower tracings in B correspond to Isc recorded during 80 min as indicated for CFBE41o- cells expressing F508del-CFTR. Isc was activated by Fsk (1 μM) and inhibited either after 10, 30, 60 and 80 min by $CFTR_{inh172}$ (10 μM). The bottom dotted line indicates the basal current level after Isc inhibition and the upper dotted line indicates the pre-activated state of Isc due to ivacaftor. F508del-CFTR cells were treated 24h with ETI. (C) quantification from multiple experiments for CF-HBE cells (left), WT- (middle) and F508del-CFTR- CFBE41o- cells (right). Data are expressed as mean ± SD (CF-HBE: 2-3 technical replicates each from 3 unique donors; CFBE41o-WT-CFTR: n=7; CFBE41o-F508del-CFTR: n=6) and compared to fsk peak in C or between two sets of data as indicated by the horizontal bar.

Figure 9. Effect of bamocaftor on Isc and protein maturation in CFBE41o-F508del-CFTR cells. (A) Representative tracings of Isc for F508del-CFTR- CFBE41o- cells treated by

ETI, BTI or BEI as indicated for each tracing. Cells were treated either by ETI (3 μM, 3μM, 1μM), BTI (3 μM, 3μM, 1μM) or BEI (3 μM, 3μM, 1μM). (B) Quantification from multiple experiments for CFBE41o- F508del-CFTR cells treated either by BTI, BEI and ETI as indicated. Data are expressed as mean ± SD (n=4). Data compared to respective basal condition. ETI data were also compared to BTI data as indicated by the horizontal bar; ****$p<0.0001$. (C) representative tracings of Isc with F508del-CFTR-CFBE41o- cells treated by three different BTI percentages as indicated for each tracing. In A and C, Isc was activated by Fsk (1 μM) and inhibited by $CFTR_{inh172}$ (10 μM). (D) Immuno-blot detection CFTR in whole lysates derived from F508del-CFTR-CFBE41o- cells treated with vehicle (DMSO) and BTI 100% (3 μM, 3μM, 1μM) and decreasing concentrations 50% and 10% BTI. Our loading control is GAPDH (bottom line). (E) Quantification of F508del-CFTR band C/(B+C) ratio from F508del-CFTR-CFBE41o- cells treated with BTI (3 μM, 3μM, 1μM) compared to ETI (3 μM, 3μM, 1μM). Data are expressed as mean ± SD (n=5-8). Data are compared to DMSO or between two sets of data as indicated by the horizontal bar. The chemical structures of elexacaftor (VX445) and bamocaftor (VX659) are presented.

Figure 10. Effect of bamocaftor on thermal instability of Isc in CFBE41o-F508del-CFTR cells. (A) original tracings of Isc with CFBE41o- F508del-CFTR cells recorded during 120 min at 37°C as indicated above tracings. Cells were treated either by ETI (3 μM, 3μM, 1μM) or BTI (3 μM, 3μM, 1μM). (B) Corresponding quantification from multiple experiments for F508del-CFTR- CFBE41o- cells treated either by BTI or ETI. The symbols a, b, c referred to the time points in A (respectively: peak; after 120'; after adding $CFTR_{inh172}$). Data are expressed as mean ± SD (n=6-8) and are compared to the respective fsk peak or between two sets of data as indicated by the horizontal bar. ****$p<0.0001$.

Figure 1

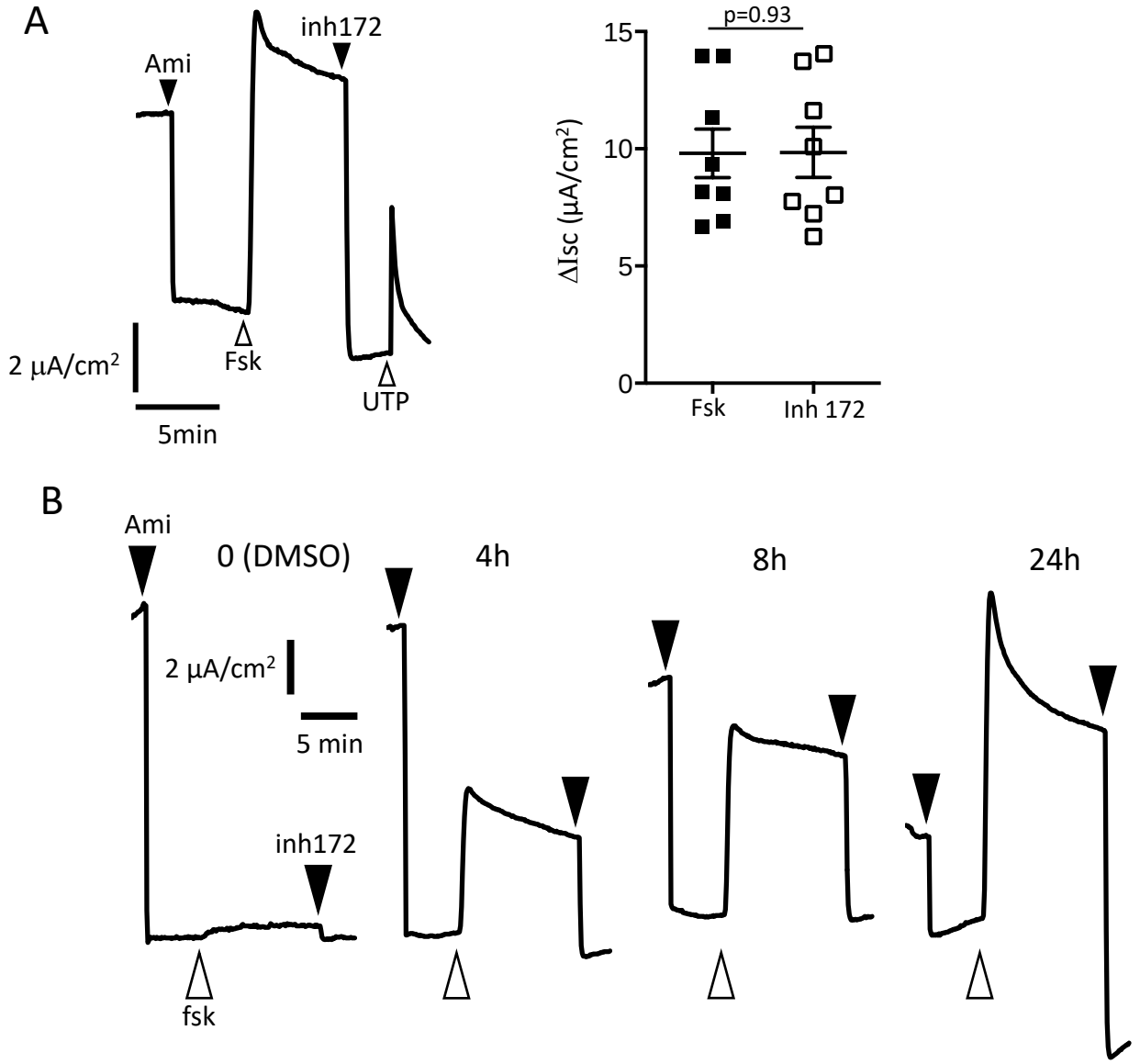

Figure 2

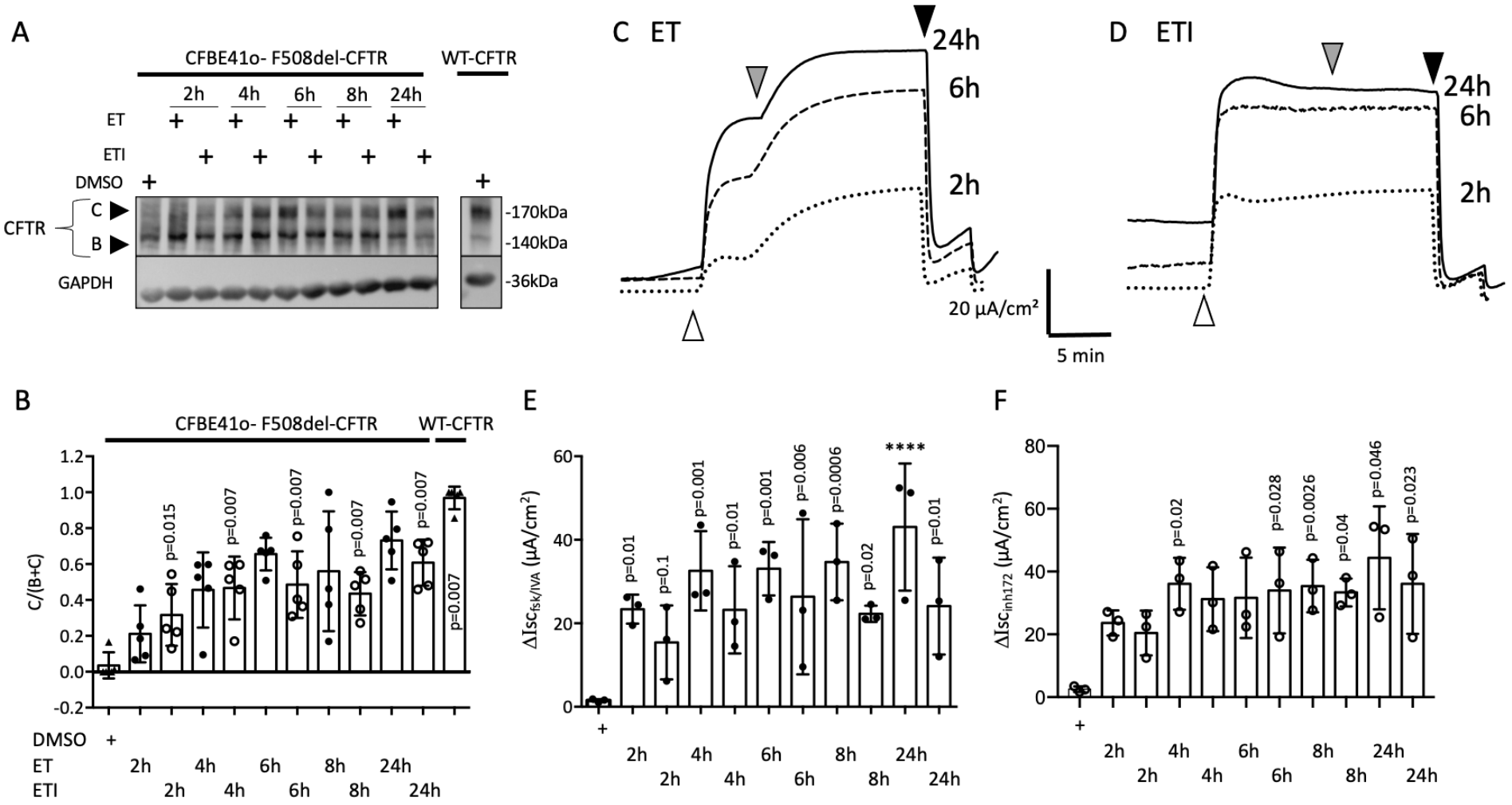

Figure 3

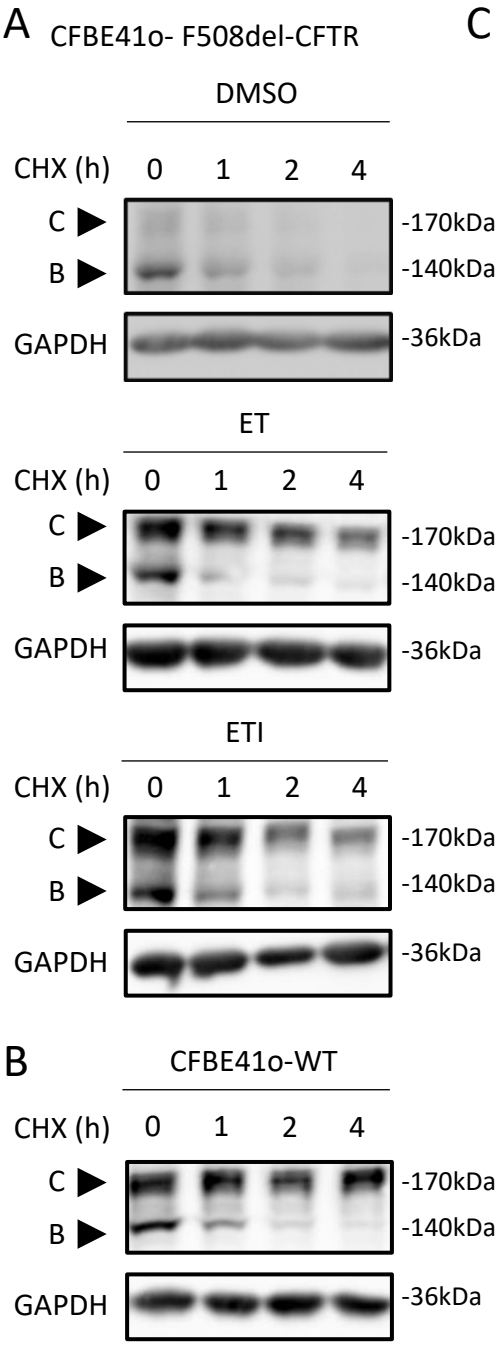

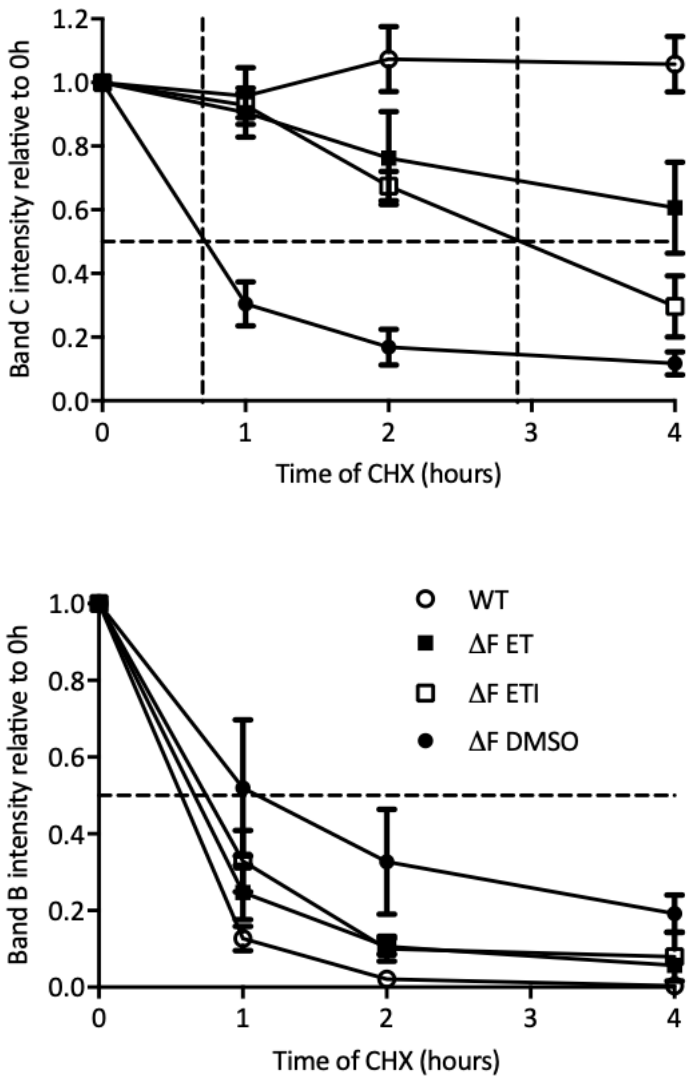

Figure 4

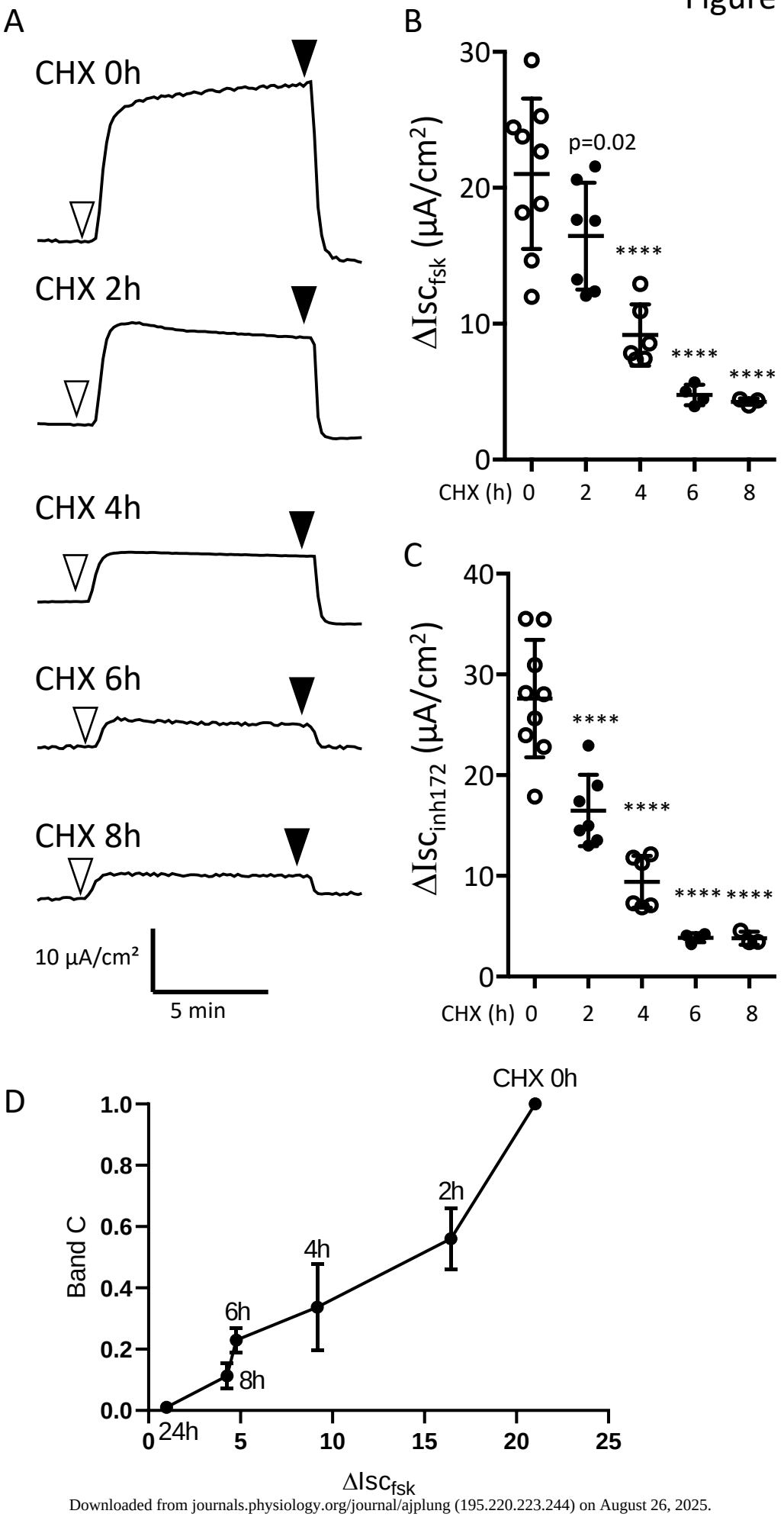

Figure 5

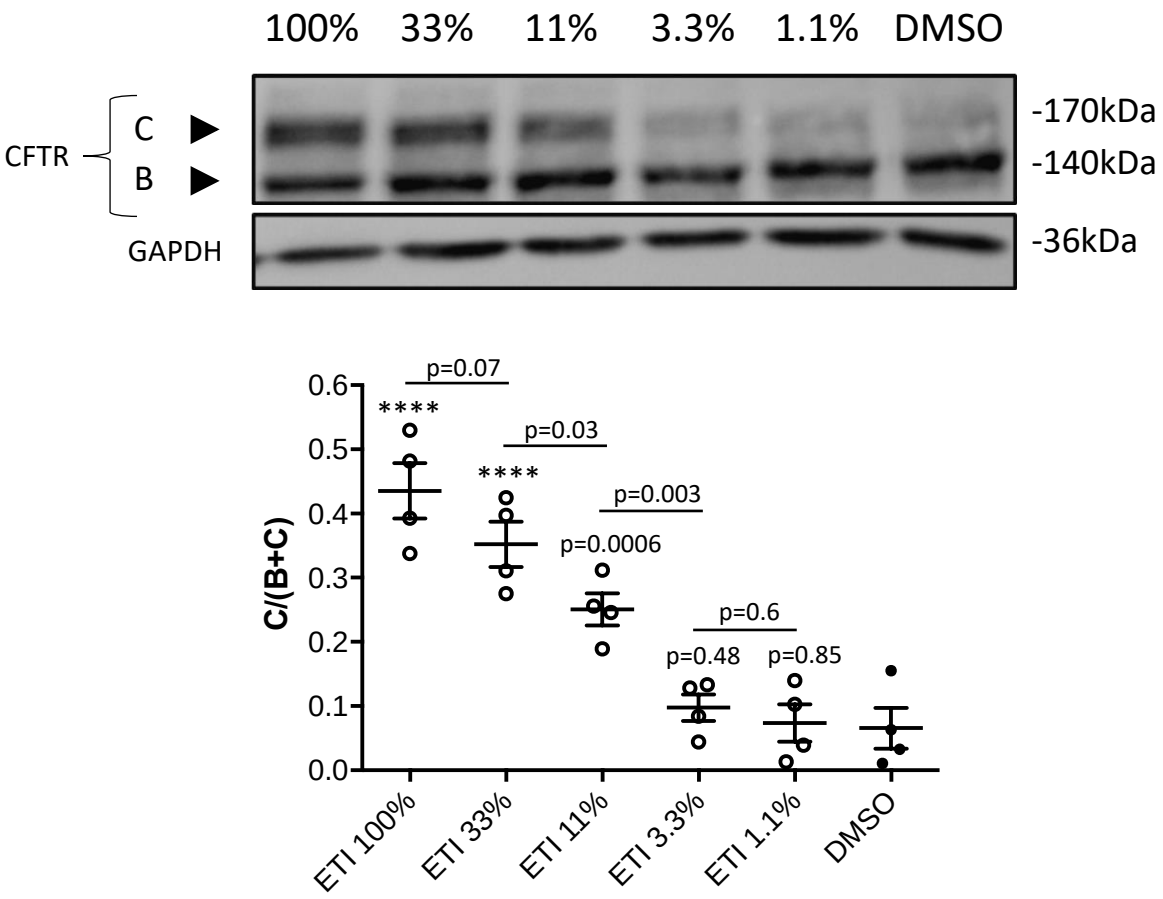

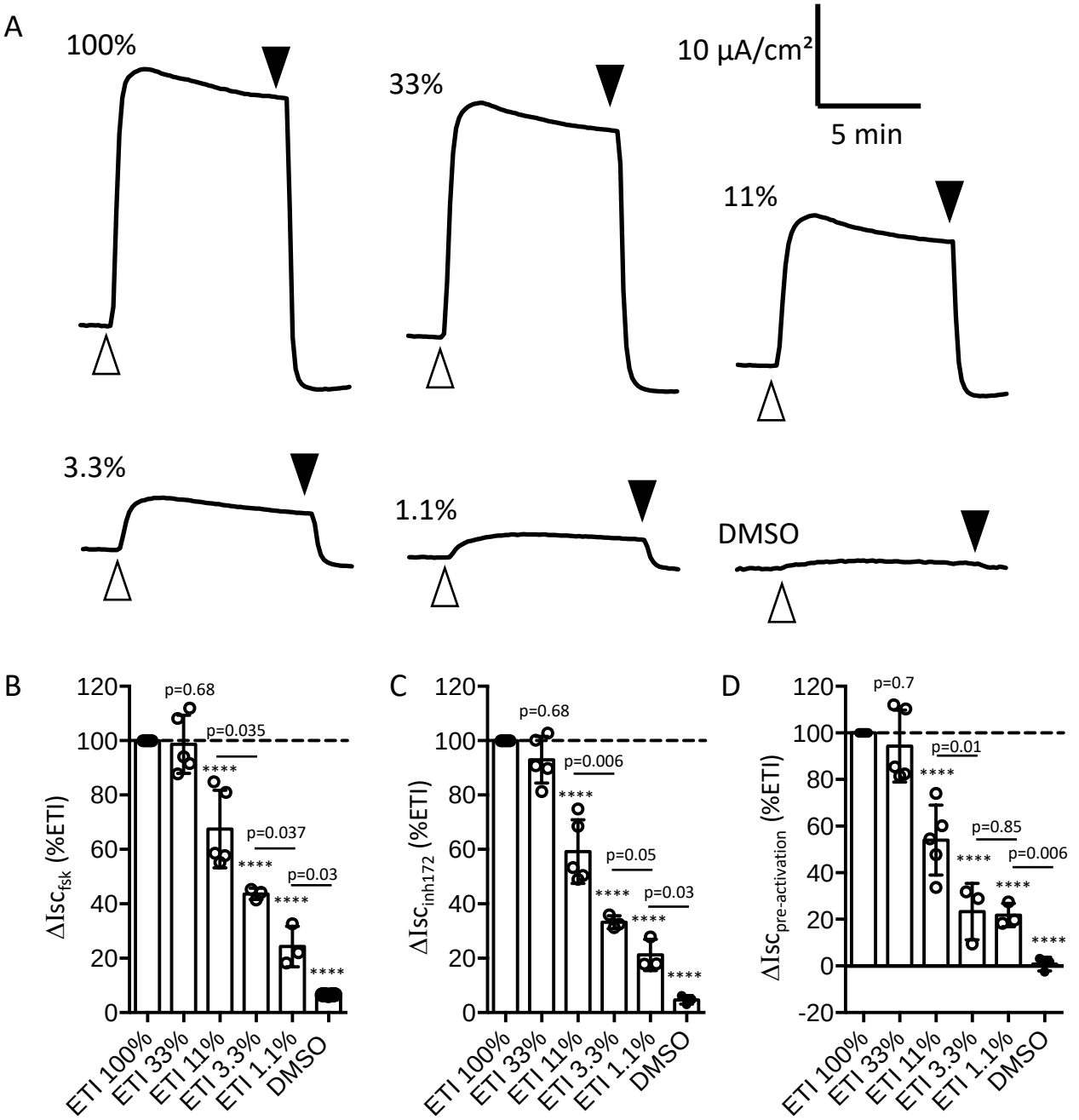

Figure 7

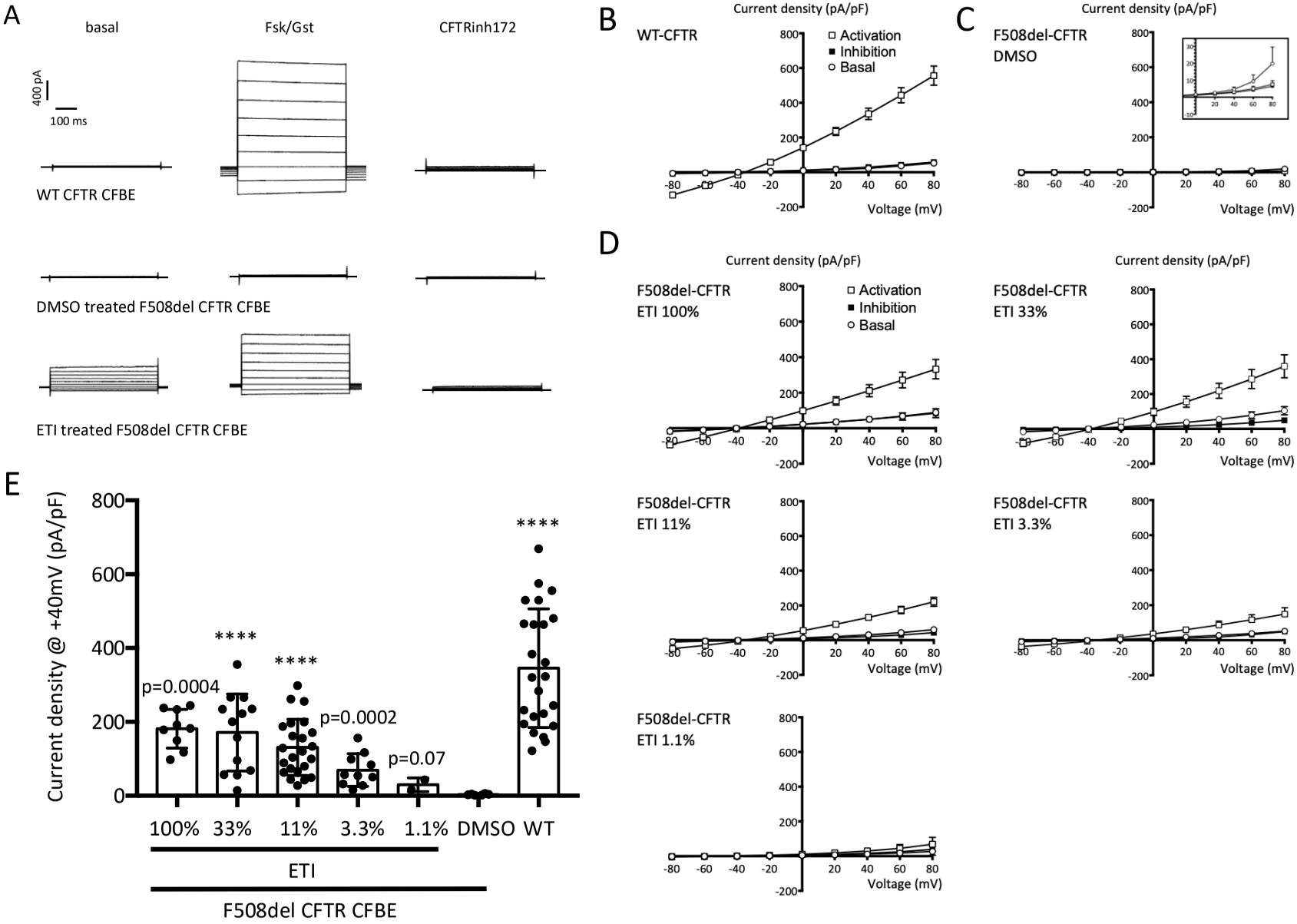

Figure 8

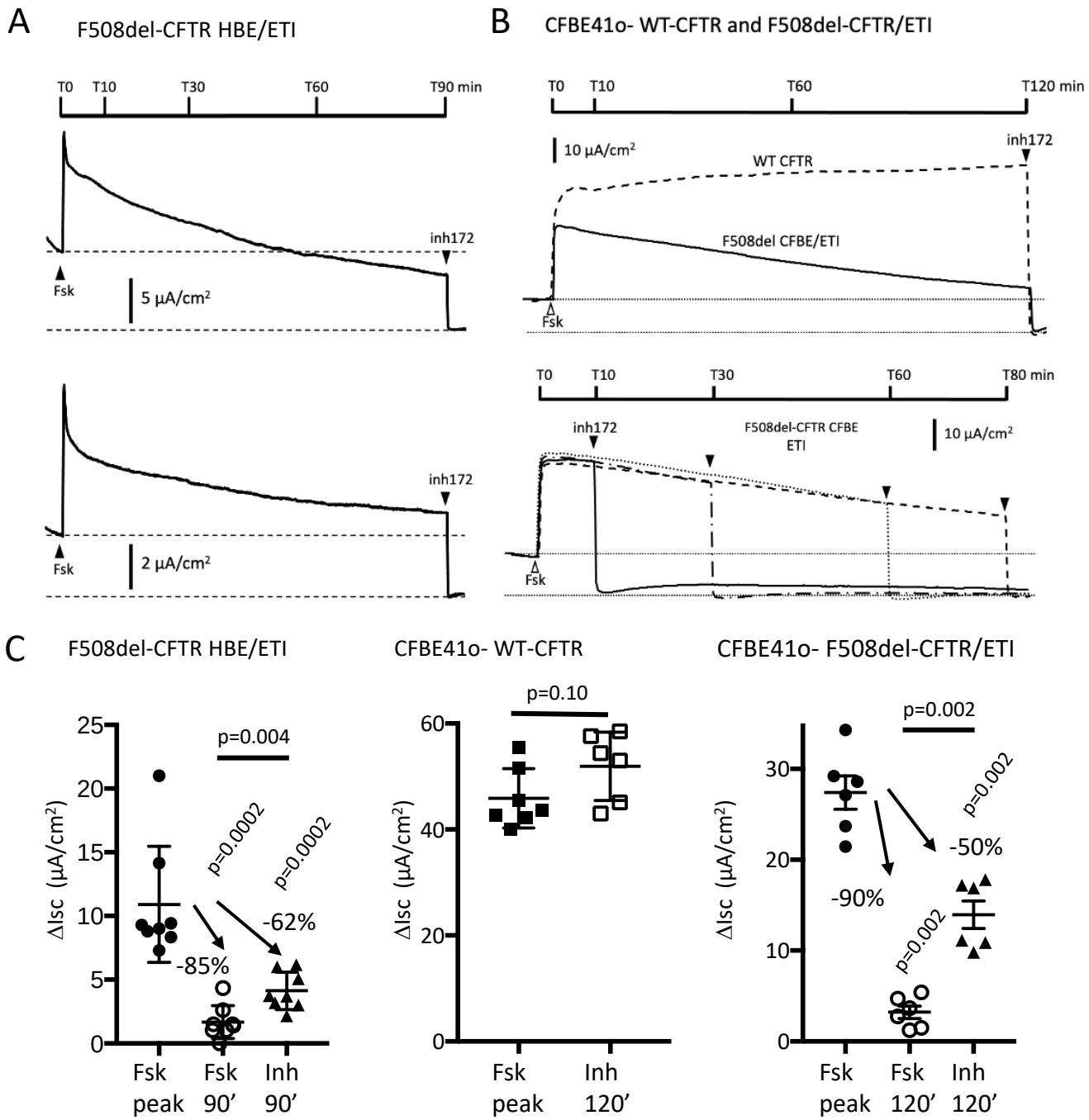

Figure 9

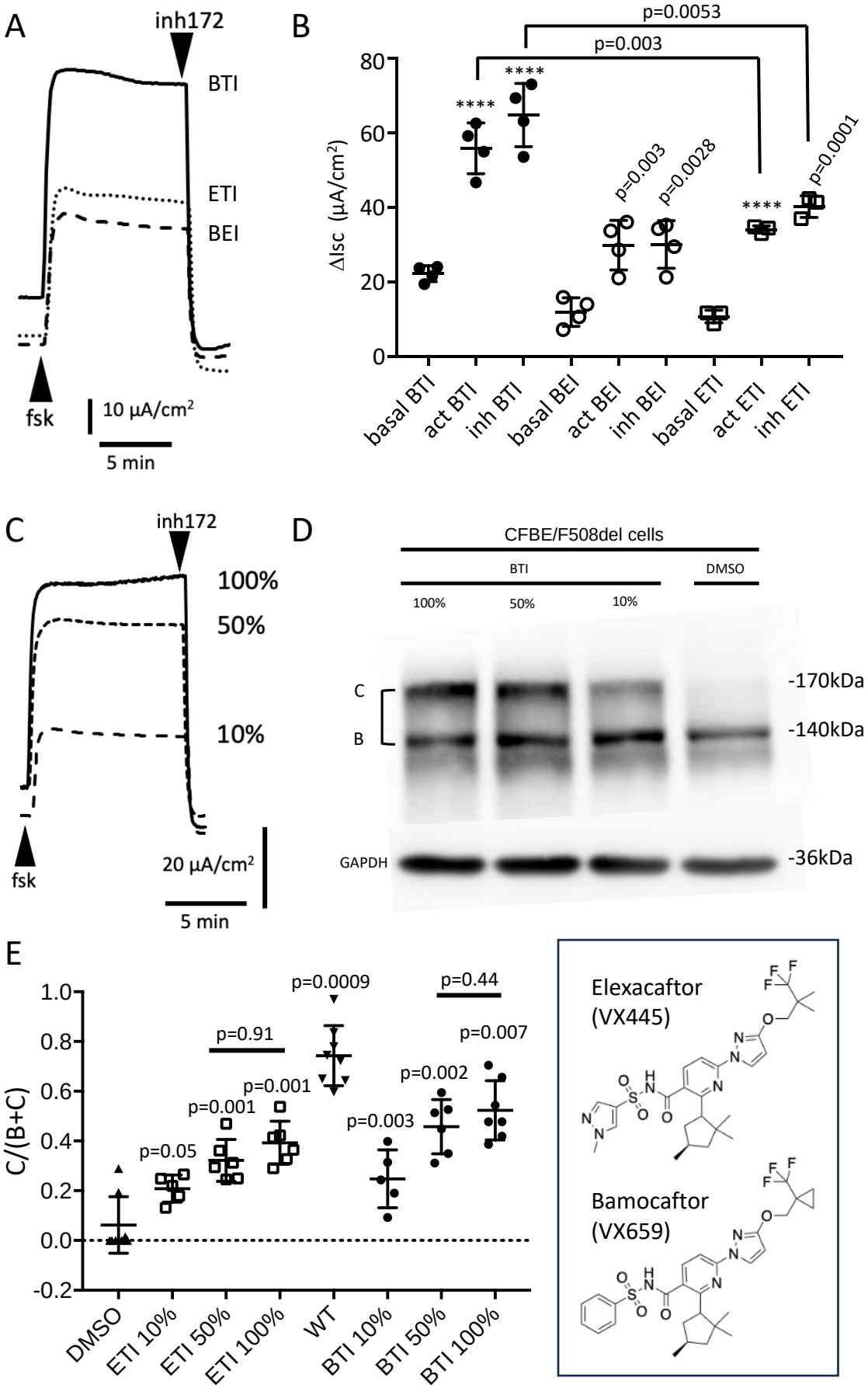

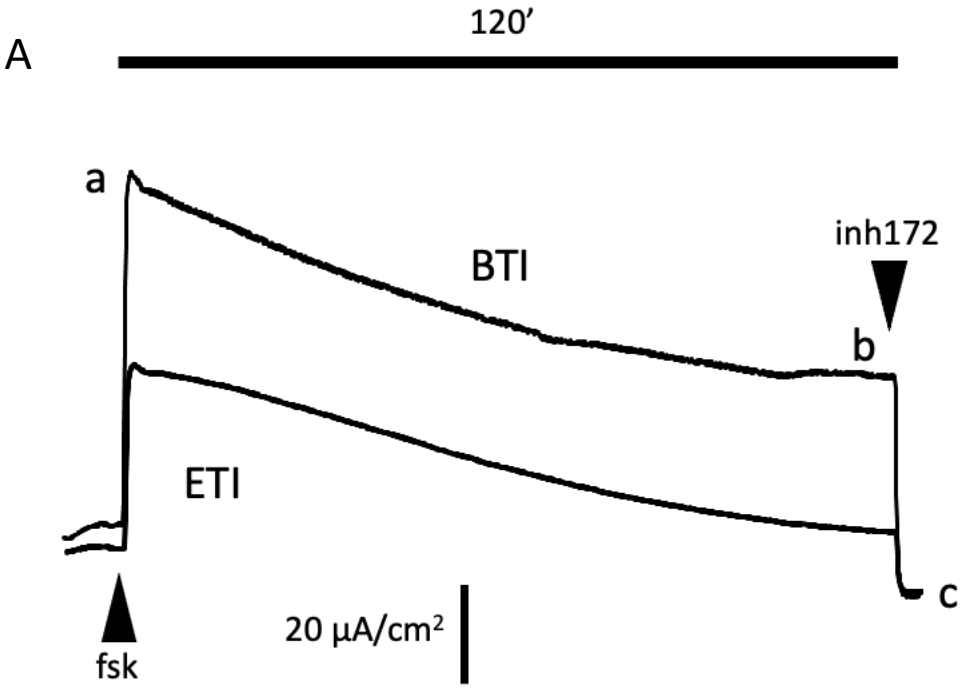

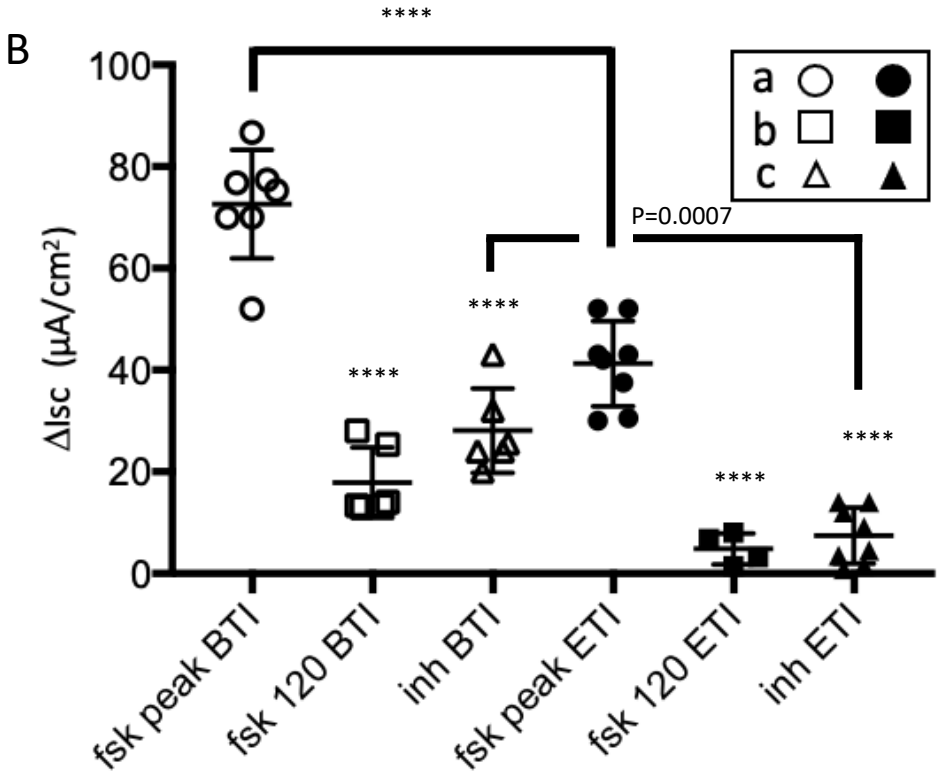

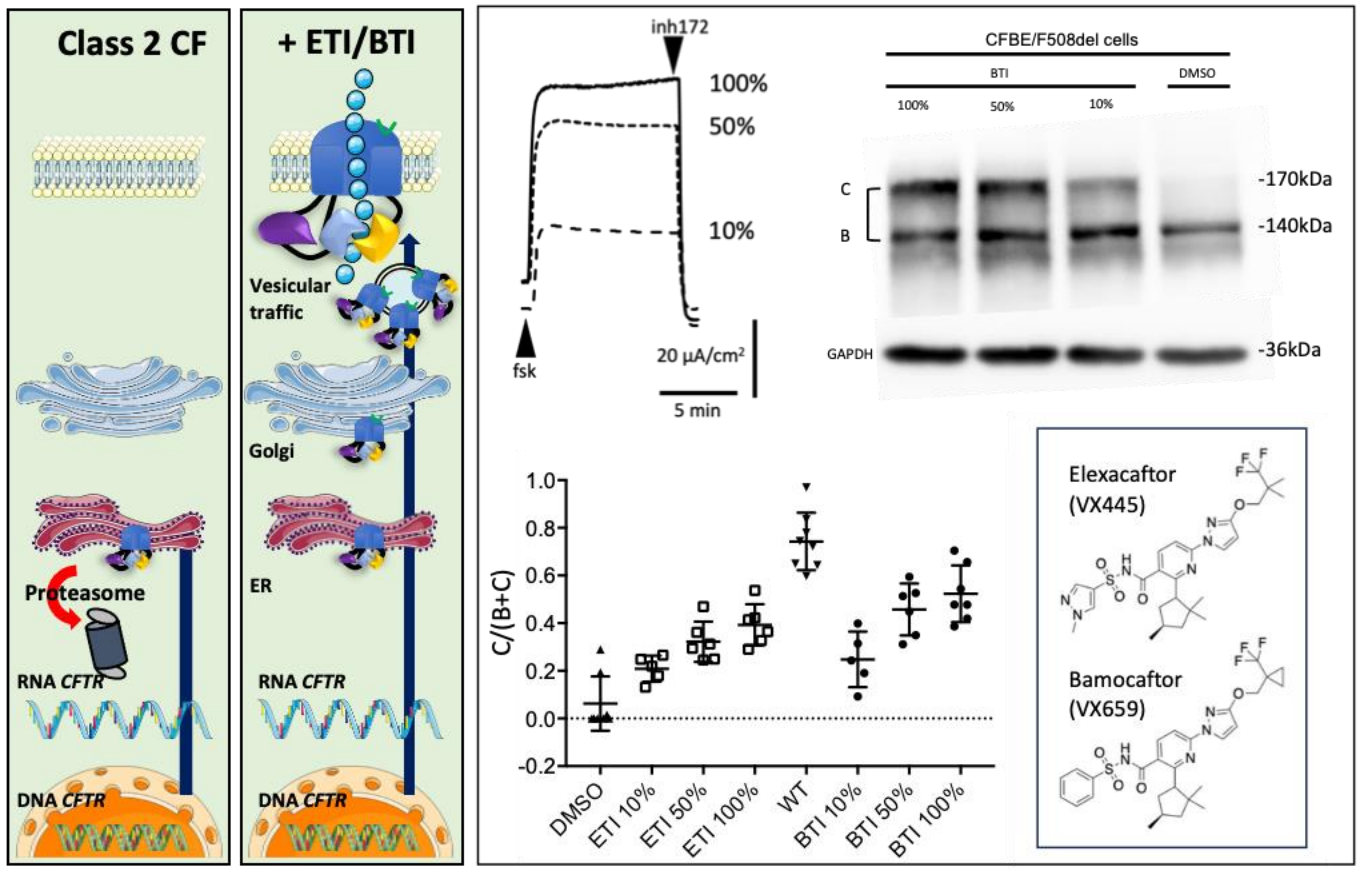

Correcting effects of elexacaftor and bamocaftor on the metabolic and thermal stability of the F508del-CFTR protein